Inorganic Chemistry

Article

pubs.acs.org/IC

Thermochemical and Mechanistic Studies of Electrocatalytic Hydrogen Production by Cobalt Complexes Containing Pendant Amines

Eric S. Wiedner,* Aaron M. Appel, Daniel L. DuBois, and R. Morris Bullock*

Center for Molecular Electrocatalysis, Physical Sciences Division, Pacific Northwest National Laboratory, P.O. Box 999, K2-57, Richland, Washington 99352, United States

Supporting Information

ABSTRACT: Two cobalt(tetraphosphine) complexes $[Co(P^{nC\text{-}PPh2}{}_2N^{Ph}{}_2)(CH_3CN)](BF_4)_2$ with a tetradentate phosphine ligand ($P^{nC\text{-}PPh2}{}_2N^{Ph}{}_2$ = 1,5-diphenyl-3,7-bis((diphenylphosphino)-alkyl)-1,5-diaza-3,7-diphosphacyclooctane; alkyl = $(CH_2)_2$, n = 2 (**L2**); $(CH_2)_3$, n = 3 (**L3**)) have been studied for electrocatalytic hydrogen production using 1:1 $[(DMF)H]^+$:DMF. A turnover frequency (TOF) of 980 s^{-1} with an overpotential at $E_{cat/2}$ of 1210 mV was measured for $[Co^{II}(L2)(CH_3CN)]^{2+}$, and a TOF of 980 s^{-1} with an overpotential at $E_{cat/2}$ of 930 mV was measured for $[Co^{II}(L3)(CH_3CN)]^{2+}$. Addition of water increases the TOF of $[Co^{II}(L2)(CH_3CN)]^{2+}$ to 18,000 s^{-1}. The catalytic wave for each of these complexes occurs at the reduction potential of the corresponding HCo^{III} complex. Comprehensive thermochemical studies of $[Co^{II}(L2)(CH_3CN)]^{2+}$ and $[Co^{II}(L3)(CH_3CN)]^{2+}$ and species derived from them by addition/removal of protons/electrons were carried out using values measured experimentally and calculated using density functional theory (DFT). Notably, $HCo^{I}(L2)$ and $HCo^{I}(L3)$ were found to be remarkably strong hydride donors, with $HCo^{I}(L2)$ being a better hydride donor than BH_4^-. Mechanistic studies of these catalysts reveal that H_2 formation can occur by protonation of a HCo^{II} intermediate, and that the pendant amines of these complexes facilitate proton delivery to the cobalt center. The rate-limiting step for catalysis is a net intramolecular isomerization of the protonated pendant amine from the nonproductive exoisomer to the productive endo isomer.

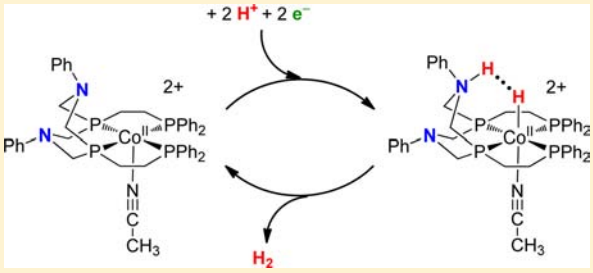

INTRODUCTION

The storage of energy in chemicals bonds is an attractive method of utilizing the electricity produced by intermittent nonfossil renewable energy sources such as wind and solar power. Molecular cobalt complexes have been studied extensively as catalysts for both electrochemical[1−20] and photochemical[3,16,19−33] H_2 production. Formation of a cobalt(III) monohydride intermediate, HCo^{III}, is typically invoked in the mechanism of these catalysts. Multiple pathways for H_2 formation from HCo^{III} have been proposed, including bimetallic and monometallic reactions at both the Co^{III} and the Co^{II} oxidation state (Scheme 1).[1,2,34−36] Computational studies have demonstrated that several pathways of H_2 formation are thermodynamically favorable.[28,34,35] The electrocatalytic mechanism has been established experimentally for several catalysts,[5,17,18] yet direct experimental mechanistic information for other catalysts remains elusive because of the high reactivity of the catalytically active HCo^{III} intermediates.[8−10,36]

We have reported cobalt complexes having a single bidentate $P^R{}_2N^{R'}{}_2$ ligand (P_2N_2 = 1,5-diaza-3,7-diphosphacyclooctane), $[Co(P^R{}_2N^{R'}{}_2)(CH_3CN)_3]^{2+}$ (**1**), that catalyze the formation of H_2 with turnover frequencies of 90−160 s^{-1}, though relatively little is known about the catalytic mechanism for these systems.[37,38] The catalytic wave for the $[Co(P^R{}_2N^{R'}{}_2)(CH_3CN)_3]^{2+}$ complexes appears at the potential of the $Co^{II/I}$ couple, which implies the Co^I species is protonated to afford a HCo^{III} complex as an intermediate. Attempts to isolate and characterize catalytic intermediates have been hindered by the propensity of these $[Co(P^R{}_2N^{R'}{}_2)(CH_3CN)_3]^{n+}$ complexes to rearrange to $[Co(P^R{}_2N^{R'}{}_2)_2(CH_3CN)]^{n+}$ complexes at either the Co^{II} oxidation state ($P^{Ph}{}_2N^{Ph}{}_2$)[38] or the Co^I oxidation state ($P^{tBu}{}_2N^{Ph}{}_2$).[39] Consequently, the chemical and electrochemical

Scheme 1. Previously Proposed Mechanisms of H_2 Formation By Cobalt Hydride Complexes

Bimetallic Mechanisms

$$2\ HCo^{III} \rightarrow 2\ Co^{II} + H_2$$

$$2\ HCo^{II} \rightarrow 2\ Co^{I} + H_2$$

Monometallic Mechanisms

$$HCo^{III} + H^+ \rightarrow Co^{III} + H_2$$

$$HCo^{II} + H^+ \rightarrow Co^{II} + H_2$$

Received: October 8, 2013
Published: November 21, 2013

processes following formation of the proposed HCo^{III} intermediate have not been observed experimentally.

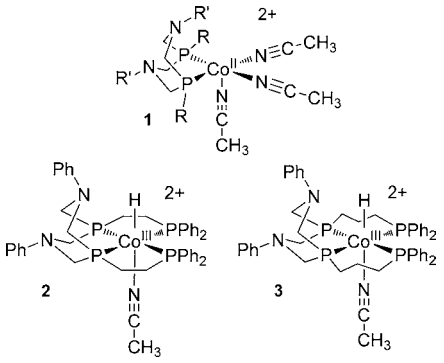

We recently reported the synthesis and isolation of the HCo^{III} complexes $[HCo^{III}(L2)(CH_3CN)]^{2+}$ (**2**) and $[HCo^{III}(L3)(CH_3CN)]^{2+}$ (**3**), which are related to the proposed $[HCo^{III}(P^R_2N^{R'}_2)(CH_3CN)_3]^{2+}$ intermediates of proton reduction by $[Co^{II}(P^R_2N^{R'}_2)(CH_3CN)_3]^{2+}$.[40] In the L2 and L3 nomenclature, the number indicates the number of carbon atoms linking the terminal phosphorus atom with the phosphorus of the cyclic P_2N_2 ligand. Electrochemical reduction of the cobalt hydrides **2** and **3** afforded a two-electron reduction from HCo^{III} to HCo^{I}, with an intervening dissociation of the acetonitrile ligand from HCo^{II}.[40] In this paper, we report the electrocatalytic activity of $[Co^{II}(L2)(CH_3CN)]^{2+}$ and $[Co^{II}(L3)(CH_3CN)]^{2+}$ for H_2 production by proton reduction, the thermochemical properties of these and related complexes, and proposed mechanisms of H_2 production.

RESULTS

Catalytic Hydrogen Production. When small quantities of $[(DMF)H]^+$ (pK_a^{MeCN} = 6.1)[41,42] were added to acetonitrile solutions of $[Co^{II}(L2)(CH_3CN)]^{2+}$, increased current indicative of a catalytic wave was observed with a half-peak potential of −1.52 V (Figure 1a). This half-peak potential is the same as the half-peak potential of −1.52 V measured for the reduction of $[HCo^{III}(L2)(CH_3CN)]^{2+}$ and indicates that reduction of this species is required for catalysis. At a $[(DMF)H]^+$ concentration of approximately 20 mM, the peak of the catalytic wave disappeared, and the catalytic current decreased, though the peak current of the initial $Co^{II/I}$ reduction was not diminished at these acid concentrations. When a 1:1 $[(DMF)H]^+$:DMF buffer solution was used as the acid, the catalytic wave was more sigmoidal in shape with a plateau at more negative potentials rather than a peak. In this case the catalytic current initially increased as the concentration of the buffered acid was increased (Figure 1b), but became independent of buffer concentration at higher concentrations (Figure 1c), as discussed next.

The mathematical expression for the peak potential (i_p) of the $Co^{II/I}$ couple in the absence of acid is given by eq 1, and the expression for the catalytic current (i_{cat}) in the presence of acid is given by eq 2.[43−47] In these equations, n' is the number of electrons (1) in the reversible $Co^{II/I}$ couple, n is the number of electrons consumed in the catalytic cycle (2 for H_2 production), R is the gas constant, T is the temperature in K, F is the Faraday constant, D is the diffusion coefficient in $cm^2\ s^{-1}$, υ is the scan rate in $V\ s^{-1}$, and k_{obs} is the observed catalytic rate constant in units of s^{-1}.[43−47] The ratio i_{cat}/i_p is described by eq 3 (n = 2 and n' = 1), and rearrangement of terms allows for calculation of k_{obs} from υ and i_{cat}/i_p at 298 K (eq 4).[43−47]

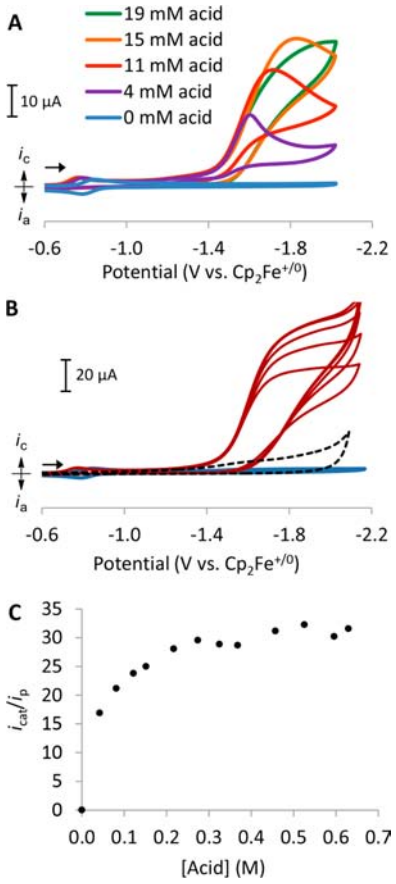

Figure 1. (a) Cyclic voltammograms of 0.5 mM $[Co^{II}(L2)(CH_3CN)]^{2+}$ with varying concentrations of $[(DMF)H]^+$, (b) cyclic voltammograms of 0.5 mM $[Co^{II}(L2)(CH_3CN)]^{2+}$ in the absence of acid (blue trace) and with varying concentrations of 1:1 $[(DMF)H]^+$:DMF (0.04−0.27 M, red traces), and 0.5 M 1:1 $[(DMF)H]^+$:DMF with no $[Co^{II}(L2)(CH_3CN)]^{2+}$ (dashed black trace), and (c) plot of i_{cat}/i_p versus 1:1 $[(DMF)H]^+$:DMF concentration. Conditions: 0.2 M NBu_4PF_6 acetonitrile solution, scan rate = 0.5 $V\ s^{-1}$, glassy carbon working electrode.

$$i_p = 0.446n'FA[\mathrm{Cat}]_T(D\upsilon)^{1/2}(n'F/RT)^{1/2} \quad (1)$$

$$i_{cat} = nFA[\mathrm{Cat}]_T(Dk_{obs})^{1/2} \quad (2)$$

$$\frac{i_{cat}}{i_p} = \frac{n}{0.4463}\sqrt{\frac{RTk_{obs}}{F\upsilon}} \quad (3)$$

$$k_{obs} = 1.94\,\upsilon\left(\frac{i_{cat}}{i_p}\right)^2 \quad (4)$$

The value of i_{cat} at each acid concentration was corrected for the background current measured in the absence of catalyst at the same acid concentration (Supporting Information, Figures S1−S2). Figure 1c shows a plot of i_{cat}/i_p vs acid concentration and indicates that the catalytic rate was initially dependent on the acid concentration and transitioned to being independent of acid concentration at high concentrations of acid. This acid concentration dependence is indicative of saturation behavior, and in the acid concentration independent region, k_{obs} corresponds to a pseudo first-order rate constant and is equivalent to the turnover frequency (TOF) of the catalyst. Using eq 4, a TOF of 980 s^{-1} was calculated for catalytic

dx.doi.org/10.1021/ic4025475 | Inorg. Chem. 2013, 52, 14391−14403

Table 1. Turnover Frequencies and Overpotentials for Proton Reduction in Acetonitrile

	[(DMF)H]$^+$:DMF 1:1 buffer				[*p*-bromoanilinium]$^+$			
complex	[acid] (M)	[H_2O] (M)	TOF[a] (s^{-1})	OP[b] (mV)	[acid] (M)	[H_2O] (M)	TOF[a] (s^{-1})	OP[b] (mV)
$[Co^{II}(L2)(CH_3CN)]^{2+}$	0.46	0.00	980	1,210	nd[c]	nd[c]	nd[c]	nd[c]
	0.52	2.10	18,000	1,270				
$[Co^{II}(L3)(CH_3CN)]^{2+}$	0.30	0.00	980	930	0.25	0.00	55[d]	710
	0.35	0.21	2,100	940	0.25	1.47	110[d]	710
$[Co^{II}(P^{Ph}{}_2N^{Ph}{}_2)(CH_3CN)_3]^{2+}$	nd[c]	nd[c]	nd[c]	nd[c]	0.20	0.00	90	430
$[Co^{II}(P^{tBu}{}_2N^{Ph}{}_2)(CH_3CN)_3]^{2+}$	nd[c]	nd[c]	nd[c]	nd[c]	0.30	0.00	160	360

[a]TOF = k_{obs} under conditions of acid concentration independence. [b]Measured at $E_{cat/2}$. [c]nd = not determined. [d]Measured in the acid concentration dependent region at [acid] = 250 mM.

hydrogen production by $[Co^{II}(L2)(CH_3CN)]^{2+}$. An overpotential of 1210 mV was determined using the potential at half-current on the catalytic wave ($E_{cat/2}$ = −1.60 V) and the thermodynamic potential for reduction of 1:1 [(DMF)H]$^+$:DMF (E°_{BH+} = −0.39 V) measured experimentally by Roberts and Bullock.[48] Similar catalytic behavior was observed as 1:1 [(DMF)H]$^+$:DMF was added to acetonitrile solutions of $[Co^{II}(L3)(CH_3CN)]^{2+}$ (Supporting Information, Figure S3), and a TOF of 980 s^{-1} was calculated for this complex in the acid concentration independent region with an overpotential at $E_{cat/2}$ of 930 mV. Hydrogen production for $[Co^{II}(L3)(CH_3CN)]^{2+}$ in the presence of 1:1 [(DMF)H]$^+$:DMF was confirmed by gas chromatographic analysis of the headspace gas obtained from a bulk electrolysis experiment; the current efficiency was determined to be 101 ± 5%.

Previous kinetic studies of $[Co^{II}(P^{Ph}{}_2N^{Ph}{}_2)(CH_3CN)_3]^{2+}$ and $[Co^{II}(P^{tBu}{}_2N^{Ph}{}_2)(CH_3CN)_3]^{2+}$ were performed using the weak acid *p*-bromoanilinium (pK_a^{MeCN} = 9.4),[49] and the turnover frequencies and overpotentials for these catalysts are listed in Table 1 for comparison.[37,38] The overpotentials listed in Table 1 for $[Co^{II}(P^{Ph}{}_2N^{Ph}{}_2)(CH_3CN)_3]^{2+}$ and $[Co^{II}(P^{tBu}{}_2N^{Ph}{}_2)(CH_3CN)_3]^{2+}$ are reported at $E_{cat/2}$ versus the thermodynamic potential for reduction of 1:1 *p*-bromoanilinium:*p*-bromoaniline (E°_{BH+} = −0.56 V) measured experimentally by Roberts and Bullock,[48] and as such they differ from the previously reported values. The direct reduction of *p*-bromoanilinium at the glassy carbon electrode overlaps significantly with the catalytic wave for proton reduction catalyzed by $[Co^{II}(L2)(CH_3CN)]^{2+}$. When *p*-bromoanilinium was added to $[Co^{II}(L3)(CH_3CN)]^{2+}$, the peak potential of the catalytic wave appeared at −1.43 V, which is sufficiently positive of the electrode catalyzed acid reduction wave (Supporting Information, Figures S4−S5) to allow the determination of meaningful rates. A plot of i_{cat}/i_p versus the square root of the acid concentration is nearly linear (Supporting Information, Figure S6), which indicates that the catalyst was operating in an acid concentration dependent regime (the presaturation regime). A value of k_{obs} = 55 s^{-1} was measured at an acid concentration of 250 mM (the presaturation regime), and an overpotential of 710 mV was determined using the difference between $E_{cat/2}$ (−1.27 V) and the thermodynamic potential for reduction of 1:1 *p*-bromoanilinium:*p*-bromoaniline (E°_{BH+} = −0.56 V).[48]

Addition of water to acetonitrile solutions of $[Co^{II}(L2)(CH_3CN)]^{2+}$ containing about 0.5 M of both dimethylformamide (DMF) and [(DMF)H]$^+$ led to large increases in the observed catalytic current (Supporting Information, Figure S7). Control experiments indicate that water does not have a significant effect on the background current in the absence of the cobalt catalyst (Supporting Information, Figures S1 and S8). A maximum current enhancement is observed at water concentrations of 2.0−3.5 M (4−6% v/v), and the catalytic current remains constant as the concentration of water is increased further. A TOF of 18,000 s^{-1} is calculated under these conditions, indicating a rate enhancement of approximately a factor of 20 in the presence of water. A more modest rate enhancement of a factor of 2 is observed when water (0.2−1.5 M) is added to acetonitrile solutions of $[Co^{II}(L3)(CH_3CN)]^{2+}$ using both 1:1 [(DMF)H]$^+$:DMF (TOF = 2100 s^{-1} with water) and *p*-bromoanilinium (k_{obs} = 110 s^{-1}, [acid] = 250 mM, with water) as the acid (Supporting Information, Figures S9−S10).

For an electrocatalytic process that is first-order in catalyst, the catalytic current is directly proportional to the concentration of the catalyst, as shown in eq 2, where *A* is the area of the electrode surface, $[Cat]_T$ is the total concentration of the catalyst, and *D* is the diffusion coefficient of the catalyst.[43−45] The catalytic current increases linearly with $[Co^{II}(L3)(CH_3CN)]^{2+}$ concentration when *p*-bromoanilinium was used as the acid (Supporting Information, Figure S11). This indicates that the rate-limiting step for proton reduction by $[Co^{II}(L3)(CH_3CN)]^{2+}$ is first-order in catalyst.

The above data are consistent with the active electrocatalyst being a homogeneous species. A "rinse" test was performed as an extra control to rule out formation of a catalytically active heterogeneous deposit. A cyclic voltammogram was recorded on an acetonitrile solution containing $[Co^{II}(L2)(CH_3CN)]^{2+}$ (0.4 mM), 1:1 [(DMF)H]$^+$:DMF (0.6 M), and H_2O (2.1 M). The potential was scanned through the catalytic wave, then the working electrode was rinsed and immersed in an acetonitrile solution containing 1:1 [(DMF)H]$^+$:DMF (0.6 M) and H_2O (2.1 M) but no $[Co^{II}(L2)(CH_3CN)]^{2+}$. No catalytic current was observed upon recording a voltammogram of the fresh solution (Supporting Information, Figure S12), which indicates that the active electrocatalyst is homogeneous.

Thermochemical Measurements. Addition of 2,4,6-trimethylpyridine (collidine) to an acetonitrile solution of $[HCo^{III}(L2)(CH_3CN)]^{2+}$ resulted in an equilibrium between $[HCo^{III}(L2)(CH_3CN)]^{2+}$ and $[Co^{I}(L2)(CH_3CN)]^{+}$ as determined by ^{1}H NMR spectroscopy (eq 5). The ratios of $[HCo^{III}(L2)(CH_3CN)]^{2+}$ and $[Co^{I}(L2)(CH_3CN)]^{+}$ were determined by integration of the PCH_2N resonances for each complex. The two methyl resonances for collidinium and collidine each coalesced into an average resonance because of fast exchange between the protonated and the deprotonated forms, and the weighted averages of the chemical shifts of the methyl groups were used to determine the ratio of acid to base. Using these data, the equilibrium constant for the deprotonation of $[HCo^{III}(L2)(CH_3CN)]^{2+}$ with collidine was determined to be 0.10 ± 0.02. The measured equilibrium constant and the pK_a value of 14.98 for collidinium in acetonitrile[49] were used to determine a pK_a value of 16.0 ± 0.4 for $[HCo^{III}(L2)$-

dx.doi.org/10.1021/ic4025475 | Inorg. Chem. 2013, 52, 14391−14403

Scheme 2. Thermochemical Data for $[Co^{II}(L2)(CH_3CN)]^{2+}$ and Related Species in Acetonitrile Solution, Showing Relationships Between $E°$, pK_a, $\Delta G°_{H\bullet}$, and $\Delta G°_{H-}$ Values[a,b]

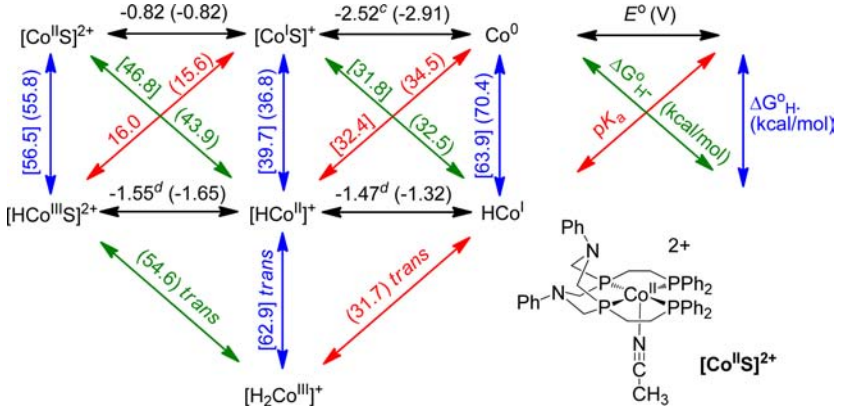

[a]S = CH_3CN ligand. [b]Unbracketed values were determined experimentally, values in [brackets] were determined by completion of a thermochemical cycle, and values in parentheses were calculated using DFT computed isodesmic reactions using $[Co^{II}(dppe)_2(CH_3CN)]^{2+}$ as a reference system. [c]Estimated from E_{pc} of the irreversible $Co^{I/-I}$ couple using the relationship $E_{1/2} = E_p + 14$ mV for a Nernstian 2-electron wave. [d]Determined by digital simulation of experimental cyclic voltammograms.

$(CH_3CN)]^{2+}$, which is less acidic than $[HCo^{III}(dppe)_2(CH_3CN)]^{2+}$ (pK_a = 11.9).[50,51]

$$[HCo^{III}(L2)(CH_3CN)]^{2+} + B \rightleftharpoons [Co^{I}(L2)(CH_3CN)]^{+} + [HB]^{+} \quad (5)$$

By employing established thermodynamic cycles,[52−57] the experimentally measured pK_a value for $[HCo^{III}(L2)(CH_3CN)]^{2+}$ and the reduction potentials of $[Co^{II}(L2)(CH_3CN)]^{2+}$, $[Co^{I}(L2)]^{+}$, $[HCo^{III}(L2)(CH_3CN)]^{2+}$, and $[HCo^{II}(L2)]^{+}$ can be used to construct the thermochemical diagram in Scheme 2.[40] This diagram illustrates the energetics of the H−Co bond in acetonitrile solution in terms of its Brønsted−Lowry acidity (pK_a), homolytic bond dissociation free energy ($\Delta G°_{H\bullet}$), and hydride donor ability ($\Delta G°_{H-}$). A value that has not been experimentally measured can be calculated when it occupies the third side of a triangle for which values of the first two sides are known (a more detailed description is given in the Supporting Information); values determined in this manner are given in [brackets] in Scheme 2. Thermodynamic properties were also calculated by DFT as discussed below, and in Scheme 2 these values are enclosed by parentheses.

Reduction of $[HCo^{III}(L2)(CH_3CN)]^{2+}$ (first column of Scheme 2) to $[HCo^{II}(L2)]^{+}$ (second column) is accompanied by loss of an acetonitrile ligand. Digital simulation of cyclic voltammograms of isolated $[HCo^{III}(L2)(CH_3CN)]^{2+}$ afforded a value of $E°$ = −1.56 V for the $[HCo^{III/II}(L2)(CH_3CN)]^{2+/+}$ couple, which does not include dissociation of the acetonitrile ligand.[40] Simulations also afforded a value of 32 M for the equilibrium constant (K_S) for acetonitrile dissociation from $[HCo^{II}(L2)(CH_3CN)]^{+}$ to give $[HCo^{II}(L2)]^{+}$ (eq 6).[40] From this equilibrium constant, $[HCo^{II}(L2)]^{+}$ is calculated to be only 0.3 kcal mol^{-1} more stable than $[HCo^{II}(L2)(CH_3CN)]^{+}$ in acetonitrile solvent, which has been estimated to have an activity of 18 M.[58] This data indicates that the $\Delta G°_{H-}$ values of $[HCo^{II}(L2)]^{+}$ and $[HCo^{II}(L2)(CH_3CN)]^{+}$ are essentially identical.

$$[HCo^{II}(L2)(CH_3CN)]^{+} \rightleftharpoons [HCo^{II}(L2)]^{+} + CH_3CN \quad K_s \quad (6)$$

A substantial amount of DMF (ca. 0.5 M) was present under the electrocatalytic conditions described above. Displacement of an acetonitrile ligand for a DMF ligand could affect the energetics of the H−Co bond. However, the potential of the $[Co^{II/I}(L2)(CH_3CN)]^{2+/+}$ couple did not change when 0.65 M DMF was added to an acetonitrile solution of $[Co^{II}(L2)(CH_3CN)]^{2+}$ (Supporting Information, Figure S13), which suggests that DMF binding is not competitive with acetonitrile binding.

The values shown in Scheme 2 were also determined computationally using a DFT protocol (see Experimental Section) that has been shown to afford thermodynamic properties for a series of $[Ni(diphosphine)_2]^{2+}$ complexes with an accuracy of 2 kcal mol^{-1}.[59] This level of computational accuracy corresponds to a maximum error of ±87 mV for calculated redox potentials ($\Delta\Delta G = 23.06 \times \Delta E°$) and ±1.5 pK_a units ($\Delta\Delta G = 1.364 \times \Delta pK_a$). A series of isodesmic reactions were constructed using $[Co^{II}(dppe)_2(CH_3CN)]^{2+}$ (dppe = 1,2-bis(diphenylphosphino)ethane) and its analogues as a reference system, since the analogous thermochemical properties of this system have been reported.[50,51] An example isodesmic reaction for transfer of H$^\bullet$ from $[HCo^{III}(L2)(CH_3CN)]^{2+}$ to $[Co^{II}(dppe)_2(CH_3CN)]^{2+}$ is given in eq 7. The value of $\Delta G°_{H\bullet}$ for $[HCo^{III}(L2)(CH_3CN)]^{2+}$ is calculated using the free energy calculated for eq 7 and the known $\Delta G°_{H\bullet}$ value for $[HCo^{III}(dppe)_2(CH_3CN)]^{2+}$.

$$[HCo^{III}(L2)(CH_3CN)]^{2+} + [Co^{II}(dppe)_2(CH_3CN)]^{2+} \rightarrow [Co^{II}(L2)(CH_3CN)]^{2+} + [HCo^{III}(dppe)_2(CH_3CN)]^{2+} \quad (7)$$

The differences between the experimental and computational values shown in Scheme 2 are as high as 9 kcal mol^{-1} ($E°$ $Co^{I/0}$), which is a considerably larger discrepancy than previously reported for this computational protocol.[59] One factor contributing to the increased error is that the peak potential of the experimentally observed irreversible, two-electron $[Co^{I}(L2)(CH_3CN)]^{+}/[Co^{-I}(L2)]^{-}$ redox couple was used as an estimate for $E°$ of the one-electron $[Co^{I}(L2)(CH_3CN)]^{+}/Co^{0}(L2)$ redox couple. This estimate contributes to a larger degree of uncertainty in the experimentally measured potential of the $Co^{I/0}$ couple, as well as the pK_a of $[HCo^{II}(L2)]^{+}$ and $\Delta G°_{H\bullet}$ of $HCo^{I}(L2)$, which are determined using this estimated $Co^{I/0}$

dx.doi.org/10.1021/ic4025475 | Inorg. Chem. 2013, 52, 14391−14403

Scheme 3. Thermochemical Data for $[Co^{II}(L3)(CH_3CN)]^{2+}$ and Related Species in Acetonitrile Solution, Showing Relationships Between $E°$, pK_a, $\Delta G°_{H\bullet}$, and $\Delta G°_{H-}$ Values[a,b]

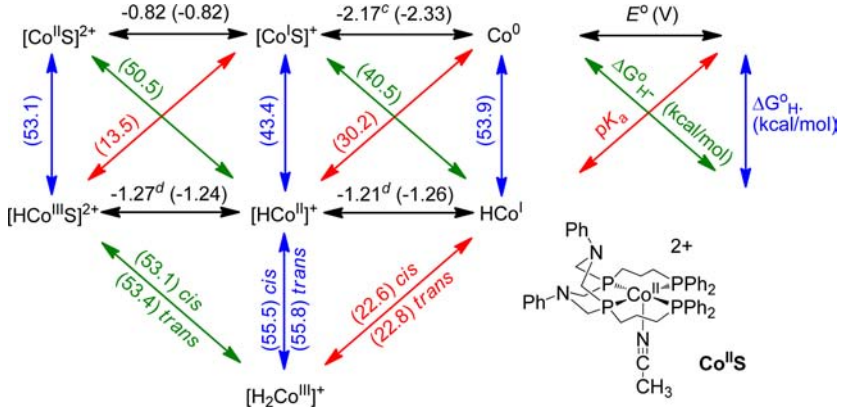

[a]S = CH_3CN ligand. [b]Unbracketed values were determined experimentally and values in parentheses () were calculated from DFT-level isodesmic reactions using $[Co^{II}(dppe)_2(CH_3CN)]^{2+}$ and its analogues as a reference system. [c]Estimated from E_{pc} of irreversible $Co^{I/0}$ couple using the relationship $E_{1/2} = E_p + 28.5$ mV for a Nernstian 1-electron wave. [d]Estimated from experimental cyclic voltammograms.

potential. Other properties exhibiting a moderate degree of computational error (2.3−3.5 kcal mol^{-1}) are $E°$ for the $[HCo^{III}(L2)(CH_3CN)]^{2+}/[HCo^{II}(L2)]^+$ and $[HCo^{II/I}(L2)]^{+/0}$ redox couples and $\Delta G°_{H-}$ and $\Delta G°_{H\bullet}$ of $[HCo^{II}(L2)]^+$. These values involve $[HCo^{II}(L2)]^+$, and the computational error may result from an inability to find the lowest-energy conformation of this complex.[59] The remaining thermodynamic quantities in Scheme 2 have a computational error of less than 2 kcal mol^{-1} ($\Delta\Delta G = 23.06 \times \Delta E°$; $\Delta\Delta G = 1.364 \times \Delta pK_a$): $E°$ of the $[Co^{II/I}(L2)(CH_3CN)]^{2+/+}$ couple, pK_a and $\Delta G°_{H\bullet}$ of $[HCo^{III}(L2)(CH_3CN)]^{2+}$, and $\Delta G°_{H-}$ of $HCo^{I}(L2)$.

Notably, this level of computational accuracy was achieved only when two criteria were met. First, reversible acetonitrile dissociation from the Co^I species must be accounted for in the isodesmic reactions. Second, each property should be determined relative to the equivalent reference property. For example, use of the $[Co^{II}(dppe)_2(CH_3CN)]^{2+}/[Co^{I}(dppe)_2]^+$ couple as a reference afforded a potential of −0.64 V for the $[HCo^{III}(L2)(CH_3CN)]^{2+}/[HCo^{II}(L2)]^+$ couple, which corresponds to a computational error of 21.0 kcal mol^{-1} (0.91 V). In contrast, using the $[HCo^{III}(dppe)_2(CH_3CN)]^{2+}/[HCo^{II}(dppe)_2]^+$ couple as a reference, a potential of −1.65 V was calculated for the $[HCo^{III}(L2)(CH_3CN)]^{2+}/[HCo^{II}(L2)]^+$ couple for a computational error of 2.3 kcal mol^{-1} (0.10 V). These findings are discussed in more detail in the Supporting Information.

Oxidative addition of H_2 to Co^I tetraphosphine or Co^I bis-diphosphine complexes is known to afford Co^{III} *cis*-dihydride complexes.[50,60−64] *Trans*-dihydride complexes of Group 9 metals are less common and are typically formed from rearrangement of the corresponding *cis*-dihydride isomers.[64−69] The coordination geometry of the tetradentate L2 ligand does not permit a *cis*-dihydride geometry, but a *trans*-dihydride structure is possible. DFT calculations were employed to determine the $\Delta G°_{H-}$ and pK_a values (see Scheme 2) of the hypothetical *trans*-dihydride complex, *trans*-$[(H)_2Co^{III}(L2)]^+$, by comparison to the reference compound *cis*-$[(H)_2Co^{III}(dppe)_2]^+$, for which $\Delta G°_{H-}$ and pK_a have been experimentally measured. The value of $\Delta G°_{H\bullet}$ for *trans*-$[(H)_2Co^{III}(L2)]^+$ was determined by construction of a thermochemical cycle using the calculated pK_a of 31.7 and the experimentally determined $[HCo^{II/I}(L2)]^{+/0}$ redox couple.

When $[HCo^{III}(L3)(CH_3CN)]^{2+}$ was treated with 2,4,6-collidine, multiple hydride resonances were observed in the ^1H NMR spectrum. As a result, the pK_a of $[HCo^{III}(L3)(CH_3CN)]^{2+}$ cannot be reliably determined because of the formation of these undesired byproducts. Therefore DFT calculations were used to provide data needed to construct a thermochemical diagram (Scheme 3) for $[Co^{II}(L3)(CH_3CN)]^{2+}$ and its analogues, using the $[Co^{II}(dppe)_2(CH_3CN)]^{2+}$ system as the reference. In this case, the computational values of the $Co^{II/I}$, $HCo^{III/II}$, and $HCo^{II/I}$ redox couples were within 90 mV (2 kcal mol^{-1}) of the experimentally observed values, while a larger error of 160 mV (3.7 kcal mol^{-1}) was obtained for the $Co^{I/0}$ couple. Accordingly, the computational pK_a, $\Delta G°_{H\bullet}$, and $\Delta G°_{H-}$ values which are based on the more accurately determined $Co^{II/I}$, $HCo^{III/II}$, and $HCo^{II/I}$ redox couples are expected to have a computational accuracy of ±2 kcal mol^{-1} for the $[Co^{II}(L3)(CH_3CN)]^{2+}$ system.

The greater flexibility of the **L3** ligand relative to the **L2** ligand suggests that protonation of $HCo^{I}(L3)$ may result in either a *cis*- or a *trans*-isomer of $[(H)_2Co^{III}(L3)]^+$. DFT calculations on these species indicate that the two isomers are nearly isoenergetic, with the *trans*-isomer being more stable by 0.3 kcal mol^{-1}. Values of $\Delta G°_{H-}$, $\Delta G°_{H\bullet}$, and pK_a for both *cis*- and *trans*-$[(H)_2Co^{III}(L3)]^+$ were calculated by DFT using *cis*-$[(H)_2Co^{III}(dppe)_2]^+$ as a reference, and these values are given in Scheme 3.

Protonation of $[HCo^{III}(L2/L3)(CH_3CN)]^{2+}$. Addition of $HBF_4{\cdot}Et_2O$ to an acetonitrile solution of $[HCo^{III}(L2)(CH_3CN)]^{2+}$ led to protonation at the pendant amine, and $[HCo^{III}(L2\text{-}H)(CH_3CN)]^{3+}$ was formed as a mixture of two isomers as determined by ^1H NMR spectroscopy. The hydride resonance of the major isomer appeared as a broad singlet at −21.8 ppm, and the NH resonance was observed at 12.2 ppm. The minor isomer is distinguished by its hydride resonance at −14.2 ppm and constitutes approximately 3% of $[HCo^{III}(L2\text{-}H)(CH_3CN)]^{3+}$ (Supporting Information, Figure S14); the ratio of these isomers did not change after 1 day in CD_3CN solution. The most likely protonation isomers of $[HCo^{III}(L2\text{-}H)(CH_3CN)]^{3+}$ are the structures in which the proton is located either exo or endo to the hydride ligand, as indicated in Scheme 4. An analogous protonated hydride complex was not observed by ^1H NMR spectroscopy when $[HCo^{III}(L3)(CH_3CN)]^{2+}$ was treated with $HBF_4{\cdot}Et_2O$; instead of $[HCo^{III}(L3\text{-}H)(CH_3CN)]^{2+}$, the ^1H NMR spectrum displayed resonances for unreacted

dx.doi.org/10.1021/ic4025475 | Inorg. Chem. 2013, 52, 14391−14403

Scheme 4. Exo- Versus Endo-Protonation of $[HCo^{III}(L2)(CH_3CN)]^{2+}$

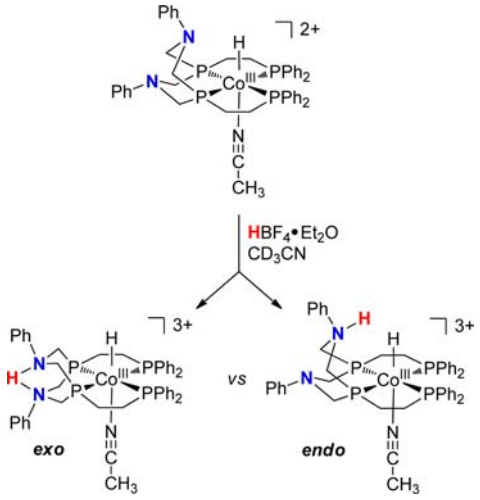

$[HCo^{III}(L3)(CH_3CN)]^{2+}$ and several new broad resonances from 10 to 5 ppm, possibly because of the formation of a paramagnetic product.

Incorporation of a ^{15}N-label into the pendant amines of $[HCo^{III}(L2\text{-}H)(CH_3CN)]^{3+}$ facilitated a structural assignment for the major isomer of this complex. The ^{15}N NMR spectrum of $[HCo^{III}(^{15}N\text{-}L2\text{-}H)(CH_3CN)]^{3+}$ contains doublets at −321.4 ppm ($^1J_{NH}$ = 39.9 Hz) and −323.1 ppm ($^1J_{NH}$ = 28.9 Hz) vs CH_3NO_2, each of which collapses to a singlet in the $^{15}N\{^1H\}$ NMR spectrum (Figure 2a). The NH resonance of $[HCo^{III}(^{15}N\text{-}L2\text{-}H)(CH_3CN)]^{3+}$ appears as a pseudotriplet that collapses into a singlet in the $^1H\{^{15}N\}$ NMR spectrum (Figure 2b), and this ^{15}N-coupled resonance can be simulated as a doublet of doublets with $^1J_{NH}$ values of 41.5 and 30.5 Hz. These ^1H and ^{15}N NMR coupling patterns demonstrate that the NH proton of the major isomer of $[HCo^{III}(L2\text{-}H)(CH_3CN)]^{3+}$ is bonded to both pendant amines of the P_2N_2 ligand fragment and is positioned exo with respect to the hydride ligand. This suggests that the minor isomer of $[HCo^{III}(L2\text{-}H)(CH_3CN)]^{3+}$ is the endo isomer, though ^{15}N resonances could not be observed for this isomer because of its low concentration relative to the exo isomer. Similar exo protonated complexes of nickel[70,71] and iron[72] have been characterized previously.

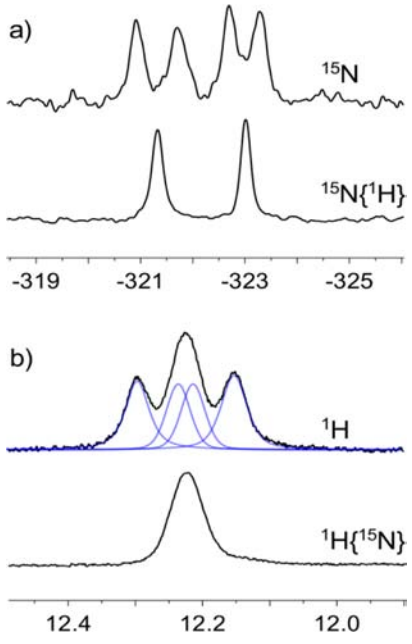

Figure 2. NMR spectra of ^{15}N-labeled *exo*-$[HCo^{III}(^{15}N\text{-}L2\text{-}H)(CH_3CN)]^{3+}$. (a) ^{15}N NMR (top trace) and $^{15}N\{^1H\}$ NMR (bottom trace) spectra, and (b) ^1H NMR (top trace, with deconvolution) and $^1H\{^{15}N\}$ NMR spectra (bottom trace) of the NHN resonance.

Addition of 2,4,6-trichloroanilinium to an acetonitrile solution of $[HCo^{III}(L2)(CH_3CN)]^{2+}$ resulted in an equilibrium between $[HCo^{III}(L2)(CH_3CN)]^{2+}$ and *exo*-$[HCo^{III}(L2\text{-}H)(CH_3CN)]^{3+}$ as shown in eq 8. An averaged signal was observed for the two cobalt species because of fast chemical exchange, and the ratio of cobalt species was determined from the weighted averages of the chemical shifts for the coordinated CH_3CN ligand. The equilibrium constant for exo protonation of $[HCo^{III}(L2)(CH_3CN)]^{2+}$ with 2,4,6-trichloroanilinium was determined to be 0.21 ± 0.04. The measured equilibrium constant and a pK_a value of 4.2 for 2,4,6-trichloroanilinium in acetonitrile (see Experimental Section) were used to determine a pK_a value of 3.5 ± 0.3 for *exo*-$[HCo^{III}(L2\text{-}H)(CH_3CN)]^{3+}$. A p$K_a$ value of 2.0 can be calculated for *endo*-$[HCo^{III}(L2\text{-}H)(CH_3CN)]^{3+}$ by using the pK_a value of *exo*-$[HCo^{III}(L2\text{-}H)(CH_3CN)]^{3+}$ and the isomer ratio of 0.03:1 (minor:major) described above; this calculation is only valid if the minor protonation isomer is the endo isomer.

$$[HCo^{III}(L2)(CH_3CN)]^{2+} + [HB]^+ \rightleftharpoons \textit{exo}\text{-}[HCo^{III}(L2\text{-}H)(CH_3CN)]^{3+} + B \quad (8)$$

Isodesmic reactions were constructed to calculate the pK_a values for the NH proton of other cobalt species in acetonitrile using *exo*-$[HCo^{III}(L2\text{-}H)(CH_3CN)]^{3+}$ as a reference, and these values are shown in Table 2. The computed pK_a of 2.3 for *endo*-$[HCo^{III}(L2\text{-}H)(CH_3CN)]^{3+}$ is similar to the pK_a of 2.0 that was predicted for this complex as described above, which supports the assignment of the minor protonation isomer as *endo*-$[HCo^{III}(L2\text{-}H)(CH_3CN)]^{3+}$. For cobalt complexes containing the **L2** ligand, the pK_a of the exo proton correlates with the total charge of the complex. The calculated pK_a of *exo*-$[HCo^{I}(L2\text{-}H)]^+$ (10.5) is very close to the pK_a value of anilinium (10.6),[49] while the average pK_a of the exo complexes with a 2+ charge is 7.4, and the average pK_a of the exo complexes containing a 3+ charge is 3.5. *Endo*-$[Co^{II}(L2\text{-}H)(CH_3CN)]^{3+}$ (pK_a = 1.8) and *endo*-$[Co^{I}(L2\text{-}H)(CH_3CN)]^{2+}$ (pK_a = 7.0) are calculated to be slightly more acidic than the corresponding *exo*-protonated isomers, while *endo*-$[HCo^{II}(L2\text{-}H)(CH_3CN)]^{2+}$ (pK_a = 10.1) and *endo*-$[HCo^{II}(L2\text{-}H)]^{2+}$ (pK_a = 10.4) are significantly less

Table 2. Computational pK_a Values in Acetonitrile Solution for NH Protons of Protonated Cobalt Complexes

	pK_a (NH)	
complex	exo	endo
$[HCo^{III}(L2\text{-}H)(CH_3CN)]^{3+}$	3.5[a]	2.3
$[Co^{II}(L2\text{-}H)(CH_3CN)]^{3+}$	3.4	1.8
$[HCo^{II}(L2\text{-}H)(CH_3CN)]^{2+}$	8.2	10.1
$[HCo^{II}(L2\text{-}H)]^{2+}$	6.5	10.4
$[Co^{I}(L2\text{-}H)(CH_3CN)]^{2+}$	7.5	7.0
$[HCo^{I}(L2\text{-}H)]^{+}$	10.5	

[a]This value was measured experimentally and was used as the reference for the DFT isodesmic reactions (and therefore matches by construction).

dx.doi.org/10.1021/ic4025475 | *Inorg. Chem.* 2013, 52, 14391−14403

acidic than *exo*-$[HCo^{II}(L2\text{-}H)(CH_3CN)]^{2+}$ (pK_a = 8.2) and *exo*-$[HCo^{II}(L2\text{-}H)]^{2+}$ (pK_a = 6.5). The lower acidity of these endo protonated hydride complexes is suggestive of a $N-H^{(\delta+)}\cdots H^{(\delta-)}-Co$ bonding interaction between the proton on the pendant amine and the hydride ligand. Similar interactions have been computed for related nickel complexes,[73,74] and these interactions are an example of a "dihydrogen" bond.[75]

Geometry optimizations on *endo*-$[HCo^{I}(L2\text{-}H)]^{+}$ resulted in the formation of $[(H_2)Co^{I}(L2)]^{+}$, containing a coordinated H_2 ligand, indicating that the hydride ligand of $HCo^{I}(L2)$ is significantly more basic than the pendant amine. Cobalt dihydrogen complexes are exceedingly rare, and to the best of our knowledge $(H_2)Co^{I}(POCOP)$ (POCOP = κ_3-C_6H_3-1,3-$[OP(tBu)_2]_2$) is the only example of a spectroscopically observable cobalt dihydrogen complex.[76] $[(H_2)Co^{I}(L2)]^{+}$ is not expected to be an experimentally observable species, and no reaction was observed between $[Co^{I}(L2)(CH_3CN)]^{+}$ and H_2 in acetonitrile solution at room temperature.

DISCUSSION

Thermodynamic Studies. It is known that the hydride donor ability of d^8 $[HM(diphosphine)_2]^{n+}$ complexes decreases (larger ΔG°_{H-} values) as the electron donor ability of the phosphorus substituents decrease and the cone angle and bite angle of the diphosphine ligand increases.[77,78] The dependence on bite angle and cone angle is a result of a distortion of the $[M(diphosphine)_2]^{(n+1)+}$ fragment from a square planar to a tetrahedral geometry, which lowers the energy of the lowest unoccupied molecular orbital (LUMO) and makes the metal fragment a better hydride acceptor.[78,79] Similarly, a distortion of $[HM(diphosphine)_2]^{n+}$ from a planar arrangement of phosphines will make the complex a weaker hydride donor. This distortion is best measured from the dihedral angle (α) that is defined by opposing P−Co−P planes, and α and ΔG°_{H-} values are given in Table 3 for a series of hydride species. The hydride complex $HCo^{I}(L2)$ is a stronger hydride donor than $HCo^{I}(L3)$ by 8.7 kcal mol^{-1} because of the smaller bite angle for **L2** than **L3**. Additionally, each of these complexes is a stronger hydride donor than $HCo^{I}(dppe)_2$[50,51] and $HCo^{I}(dedpe)_2$ (dedpe = $Et_2PCH_2CH_2PPh_2$).[64] $HCo^{I}(L2)$ is even a stronger hydride donor than $HCo^{I}(dmpe)_2$ (dmpe = $Me_2PCH_2CH_2PMe_2$), which contains a small electron rich diphosphine ligand.[64,80] The hydride donor ability of $HCo^{I}(L2)$ (ΔG°_{H-} = 31.8 kcal mol^{-1}) is between that of BH_4^- (ΔG°_{H-} > 37 kcal mol^{-1})[64] and Et_3BH^- ($\Delta G^{\circ}_{H-} \approx 26$ kcal mol^{-1}).[81,82] Transition metal hydrides that are such powerful hydride donors have only rarely been quantified by experimental methods. To the best of our knowledge, $HRh^{I}(diphosphine)_2$ complexes are the only transition metal hydride complexes that have been experimentally determined to be stronger hydride donors than $HCo^{I}(L2)$.[81,83]

Table 3. Dihedral Angles and Hydride Donor Abilities for Hydride Species

compound	α (deg)[a]	ΔG°_{H-} (kcal mol^{-1})	ref
$HCo^{I}(L2)$	17.9	31.8	this work
$HCo^{I}(L3)$	59.6	40.5	this work
$HCo^{I}(dppe)_2$	89.2	50.0	50, 51
$HCo^{I}(dedpe)_2$	81.1	46	64
$HCo^{I}(dmpe)_2$	82−84	36−37	64, 80
BH_4^-		>37	64
Et_3BH^-		≈26	81, 82
$[HCo^{II}(L2)]^{+}$	3.3	46.8	this work
$[HCo^{II}(L3)]^{+}$	66.8	50.5	this work
$[HCo^{II}(dppe)_2]^{+}$	85.9	60.6	50, 51
$[HNi^{II}(P^{Ph}{}_2N^{Ph}{}_2)_2]^{+}$		59.0	84

[a]Dihedral angle defined by opposing P−Co−P planes.

A similar relationship between α and ΔG°_{H-} is observed for the HCo^{II} complexes $[HCo^{II}(L2)]^{+}$, $[HCo^{II}(L3)]^{+}$, and $[HCo^{II}(dppe)_2]^{+}$.[50,51] While these HCo^{II} complexes are significantly weaker hydride donors than their HCo^{I} counterparts by 10−20 kcal mol^{-1}, hydride transfer from $[HCo^{II}(L2)]^{+}$ and $[HCo^{II}(L3)]^{+}$ is still very favorable within the context of electrocatalytic H_2 production. For comparison, the well-known H_2 production electrocatalyst $[Ni(P^{Ph}{}_2N^{Ph}{}_2)_2(CH_3CN)]^{2+}$ has a hydride donor ability of ΔG°_{H-} = 59.0 kcal mol^{-1}.[84]

As noted above, many Co^{I} tetraphosphine or Co^{I} bis-diphosphine complexes react with H_2 to afford Co^{III} *cis*-dihydride complexes.[50,60−64] Using the homolytic bond dissociation free energies in Scheme 3 and a free energy of 103.6 kcal mol^{-1} for the homolytic cleavage of H_2 in acetonitrile,[52] H_2 addition to $[Co^{I}(L3)(CH_3CN)]^{+}$ to form *cis*-$[(H)_2Co^{III}(L3)]^{+}$ is predicted to be endergonic (ΔG°_{H2} = +4.7 kcal mol^{-1}). A value of ΔG°_{H2} = −5.1 kcal mol^{-1} for *cis*-$[(H)_2Co^{III}(dppe)_2]^{+}$ has been determined experimentally.[50,51] No reaction is observed when an acetonitrile solution of $[Co^{I}(L3)(CH_3CN)]^{+}$ was exposed to an atmosphere of H_2, which is in agreement with computational results. The large ΔG°_{H2} value for *cis*-$[(H)_2Co^{III}(L3)]^{+}$ results from the rigidity of the L3 ligand, which cannot readily accommodate a cis-octahedral geometry. The molecular strain of *cis*-$[(H)_2Co^{III}(L3)]^{+}$ is highlighted by the dihedral angle of α = 66.6° calculated by DFT. In comparison, *cis*-$[(H)_2Co^{III}(dppe)_2]^{+}$ has a dihedral angle of α = 86.7°, which is close to the value of 90° expected for an ideal *cis*-octahedral geometry. As a result, the calculated H−H distance for *cis*-$[(H)_2Co^{III}(L3)]^{+}$ (1.794 Å) is shorter than for *cis*-$[(H)_2Co^{III}(dppe)_2]^{+}$ (1.999 Å), and H_2 release from $[(H)_2Co^{III}(L3)]^{+}$ is thermodynamically favorable.

$$[Co^{I}(L3)(CH_3CN)]^{+} + H_2 \rightleftharpoons \textit{cis}\text{-}[(H)_2Co^{III}(L3)]^{+} \quad \Delta G^{\circ}_{H2} \tag{9}$$

Mechanistic Considerations for Electrocatalysis. The appearance of the catalytic waves at the reduction potentials of $[HCo^{III}(L2)(CH_3CN)]^{2+}$ and $[HCo^{III}(L3)(CH_3CN)]^{2+}$ indicate these reductions initiate the catalytic cycles. Digital simulations of the cyclic voltammograms of $[HCo^{III}(L2)(CH_3CN)]^{2+}$ in acetonitrile in the absence of added acid are consistent with an ECE mechanism of reduction (Scheme 5), wherein the rate constant for CH_3CN dissociation from $[HCo^{II}(L2)(CH_3CN)]^{+}$ is 1000 s^{-1}, and a second electron transfer to $[HCo^{II}(L2)]^{+}$ generates $HCo^{I}(L2)$.[40] An analogous ECE reduction mechanism is proposed for $[HCo^{III}(L3)(CH_3CN)]^{2+}$, and a scan rate dependence study of this complex suggests that the rate constant for CH_3CN dissociation from $[HCo^{II}(L3)(CH_3CN)]^{+}$ is similar to the value of 1000 s^{-1} that was measured for $[HCo^{II}(L2)(CH_3CN)]^{+}$.[40] The thermodynamic values in Schemes 2 and 3 reveal that there are multiple energetically downhill pathways for electrocatalytic H_2 formation from both HCo^{II} and HCo^{I}. The possible mechanisms can be divided into two classes: a bimetallic reaction between two cobalt hydride species and a monometallic reaction between a cobalt hydride complex and an acid. While there is a strong driving force for bimetallic H_2 formation from multiple combinations of the electrochemically accessible cobalt hydride complexes, digital simulations on cyclic voltammograms of $[HCo^{III}(L2)-$

dx.doi.org/10.1021/ic4025475 | Inorg. Chem. 2013, 52, 14391−14403

Scheme 5. Proposed Mechanism for Reduction of $[HCo^{III}(L2)(CH_3CN)]^{2+}$ in the Absence of Acid

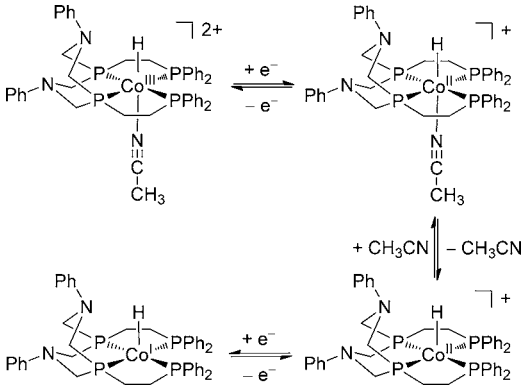

$(CH_3CN)]^{2+}$ recorded in the absence of acid indicate that bimetallic reactions of HCo^{II} and HCo^{I} do not occur on the voltammetry time scale.[40] Therefore a bimetallic mechanism of H_2 formation does not appear to be operative for either $[Co^{II}(L2)(CH_3CN)]^{2+}$ or $[Co^{II}(L3)(CH_3CN)]^{2+}$ under electrocatalytic conditions, and monometallic routes of H_2 formation are expected to predominate.

Both $[HCo^{II}(L2)(CH_3CN)]^{+}$ and $HCo^{I}(L2)$ are strong hydride donors, so each of these species is capable of generating H_2 under acidic conditions. The hydride donor strengths of these HCo^{II} and HCo^{I} species is further highlighted by voltammetry experiments in which the $[HCo^{III}(L2)(CH_3CN)]^{2+}$ reduction wave becomes irreversible in the presence of added water,[40] which is a weak Brønsted-Lowry acid in acetonitrile solution. Acetonitrile dissociation from $[HCo^{II}(L2)(CH_3CN)]^{+}$ is required for reduction to $HCo^{I}(L2)$, as shown in Scheme 5. Consequently, the mechanism of H_2 production will depend on whether protonation of $[HCo^{II}(L2)(CH_3CN)]^{+}$ (or $[HCo^{II}(L3)(CH_3CN)]^{+}$) is faster than acetonitrile ligand dissociation, which is followed by rapid reduction to $HCo^{I}(L2)$ by the electrode.

The TOF for H_2 production by $[Co^{II}(L2)(CH_3CN)]^{2+}$ in the presence of 0.5 M $[(DMF)H]^{+}$:DMF and 3.0 M water is 18,000 s^{-1}, which is significantly faster than the dissociation rate constant of 1,000 s^{-1} for loss of acetonitrile. This precludes the loss of acetonitrile from $[HCo^{II}(L2)(CH_3CN)]^{+}$ as a step in the catalytic cycle under these conditions, and therefore, electrocatalytic H_2 production is proposed to occur by protonation of $[HCo^{II}(L2)(CH_3CN)]^{+}$ (Scheme 6). The catalytic cycle is initiated by reduction of Co^{II} to Co^{I} (step 1), which can then be protonated at a pendant amine in a position that is endo with respect to cobalt, forming *endo*-Co^{I} (step 2_{endo}). The endo proton of *endo*-Co^{I} will undergo a rapid intramolecular proton transfer from nitrogen to cobalt to form HCo^{III} (step 3), which is followed by a one electron reduction to HCo^{II} (step 4) and endo protonation at a pendant amine to give *endo*-HCo^{II} (step 5_{endo}). The *endo*-HCo^{II} isomer can form an H−H bond by heterocoupling of the proton from the pendant amine and the hydride on the metal, followed by or in concert with H_2 loss to generate Co^{II} (step 6) and complete the electrocatalytic cycle.

The driving force for H_2 evolution from *endo*-HCo^{II} ($-\Delta G^{\circ}_{H2}$ = −15.7 kcal mol^{-1}) can be determined through a thermochemical cycle using ΔG°_{H-} for HCo^{II} (46.5 kcal mol^{-1}), the acid strength of the protonated pendant amine of *endo*-HCo^{II} (pK_a = 10.1, ΔG°_{H+} = 1.364 × pK_a = 13.8 kcal mol^{-1}), and a free energy of 76.0 kcal mol^{-1} for the heterolytic cleavage of H_2 in acetonitrile (Scheme 7).[52] This H−H bond formation step provides a significant driving force for the overall catalytic reaction. This step is thought to be very fast based on DFT calculations on Ni systems[85] and the experimentally observed rates of NH-MH exchange for similar manganese (>10^7 s^{-1}) and iron (>10^4 s^{-1}) systems.[86,87] The Co^{II} species produced upon loss of H_2 can be reduced at a potential of −0.82 V to form Co^{I}. However, the catalytic cycle requires reduction of HCo^{III} at −1.56 V,[40] and the reduction of Co^{II} to Co^{I} during catalysis is

Scheme 6. Proposed Electrocatalytic Cycle for H_2 Production by $[Co^{II}(L2)(CH_3CN)]^{2+}$ with 1:1 $[(DMF)H]^{+}$:DMF and H_2O

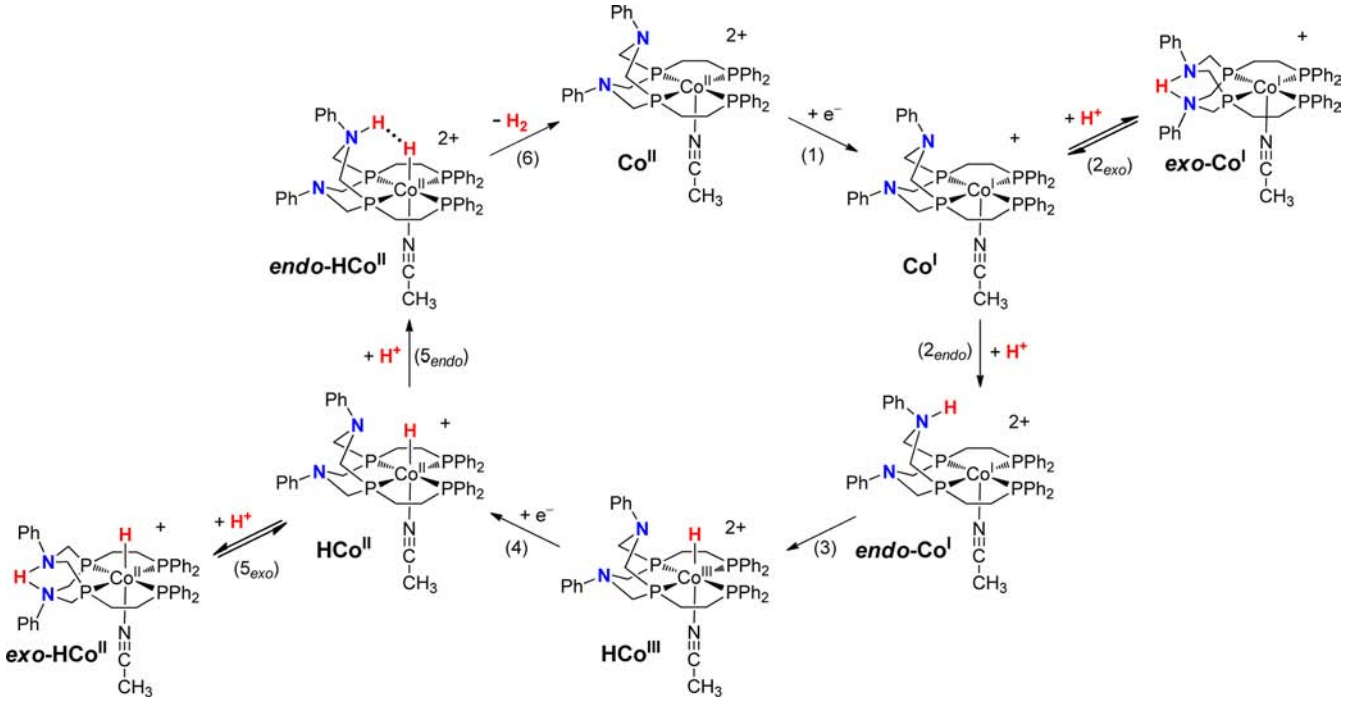

dx.doi.org/10.1021/ic4025475 | *Inorg. Chem.* 2013, 52, 14391−14403

Scheme 7. Thermochemical Cycle for Determination of $-\Delta G°_{H2}$

$[HCo^{II}(L2)(CH_3CN)]^+ \longrightarrow [Co^{II}(L2)(CH_3CN)]^{2+} + H^-$	$\Delta G°_{H-}$
$[HCo^{II}(L2\text{-}H)(CH_3CN)]^{2+} \longrightarrow [HCo^{II}(L2)(CH_3CN)]^+ + H^+$	$\Delta G°_{H+} = 1.364 \times pK_a$
$H^+ + H^- \longrightarrow H_2$	$\Delta G° = -76.0$ kcal mol^{-1}
$[HCo^{II}(L2\text{-}H)(CH_3CN)]^{2+} \longrightarrow [Co^{II}(L2)(CH_3CN)]^{2+} + H_2$	$\Delta G°_{H2}$

exergonic by 17.8 kcal mol^{-1} because of these large negative potentials.

The pK_a values of *endo*-Co^I and *endo*-HCo^{II} are calculated to be 7.0 and 10.1 while the experimentally determined value of the pK_a of $[(DMF)H]^+$ is 6.1,[41] suggesting that sufficient driving force should exist for nearly complete protonation of the reduced catalyst at high acid concentrations. Previous studies of Ni catalysts have indicated exo protonation is kinetically preferred over endo protonation,[88] and the protonation of HCo^{III} to form *exo*-HCo^{III} suggests that exo protonation of HCo^{II} to form the *exo*-HCo^{II} isomer (step 5_{exo}) is kinetically preferred over formation of *endo*-HCo^{II}. Likewise, exo protonation of Co^I to form *exo*-Co^I (step 2_{exo}) is kinetically preferred over formation of *endo*-Co^I. The *exo*-Co^I and *exo*-HCo^{II} isomers represent noncatalytic isomers that must convert to the *endo*-Co^I and *endo*-HCo^{II} isomers before catalysis can occur. While each isomerization is a net intramolecular exchange process, it occurs through an intermolecular deprotonation of the exo proton by DMF, followed by reprotonation at the endo position to afford *endo*-Co^I or *endo*-HCo^{II}.[88] This conversion of the exo to the endo protonated isomers is thought to be rate-determining at high concentrations of 1:1 $[(DMF)H]^+$:DMF. Water is believed to lower the barriers for the endo protonation (steps 2_{endo} and 5_{endo}) by serving as an intermolecular proton relay between the external acid substrate and the pendant amine.[89,90] This reduces the unfavorable steric interactions between the acid and the ligands, resulting in a faster exo to endo isomerization and a higher TOF in the presence of water.

The previous discussion has examined the mechanism in cases where the observed rate of catalysis is much faster than the rate of acetonitrile dissociation from $[HCo^{II}(L2)(CH_3CN)]^+$, and HCo^I(L2) can be excluded from mechanistic consideration. When a 1:1 $[(DMF)H]^+$:DMF buffer is used as the proton source in the absence of added H_2O for either $[Co^{II}(L2)(CH_3CN)]^{2+}$ or $[Co^{II}(L3)(CH_3CN)]^{2+}$, the TOF of each catalyst (980 s^{-1}) is approximately equal to the rate of acetonitrile dissociation from $[HCo^{II}(L2)(CH_3CN)]^+$ (1000 s^{-1}). Under these conditions, HCo^I could form as an intermediate if endo protonation of HCo^{II} (step 5_{endo}) is slow; this potential electrocatalytic cycle is depicted in the Supporting Information, Scheme S1. A second mechanistic possibility under these conditions is that endo protonation of HCo^{II} (step 5_{endo}) is more rapid than formation of HCo^I. In this case, conversion of *exo*-Co^I to *endo*-Co^I would be rate-limiting for catalysis. Both of these mechanisms are plausible under these conditions, and cannot be distinguished from the current data. However, the formation of HCo^I is consistent with electrocatalytic experiments employing unbuffered $[(DMF)H]^+$ as the acid, where the catalytic current begins to diminish at relatively low concentrations of $[(DMF)H]^+$ (ca. 20 mM). With low concentrations of base, acetonitrile dissociation could result in the formation of *exo*-$[HCo^I(L2)]^+$ which is unlikely to be isomerized to a catalytically active isomer because of the high pK_a of the exo proton (10.5).

An acid concentration independent region was not observed for the production of H_2 using $[Co^{II}(L3)(CH_3CN)]^{2+}$; k_{obs} is 55 s^{-1} with *p*-bromoanilinium at a concentration of 0.25 M. With a pK_a value of 9.4, *p*-bromoanilinium is not sufficiently acidic to fully protonate either $[Co^I(L3)(CH_3CN)]^+$ or $[HCo^{II}(L3)(CH_3CN)]^+$ to form *exo*-Co^I or *exo*-HCo^{II}, each of which has a pK_a of approximately 7.5. With a *p*-bromoanilinium concentration of 0.25 M, electrocatalytic H_2 production is slower (k_{obs} = 55 s^{-1}) than the estimated rate of acetonitrile dissociation from $[HCo^{II}(L3)(CH_3CN)]^+$ (1000 s^{-1}). These observations strongly suggest that HCo^I(L3) is an intermediate under these conditions and H_2 formation occurs by protonation of HCo^I(L3); this alternative mechanism is given in Supporting Information, Scheme S1. However, a mechanism in which protonation of $[HCo^{II}(L3)(CH_3CN)]^+$ (step 5_{endo}) is significantly faster than protonation of $[Co^I(L3)(CH_3CN)]^+$ (step 2_{endo}) is also consistent with the data and cannot be ruled out.

Comparison to Other Cobalt Electrocatalysts. Several recent mechanistic studies have proposed that a likely pathway for electrocatalytic H_2 formation in the presence of moderate to strong acids occurs by reduction of a HCo^{III} intermediate and protonation of the resulting HCo^{II} species to generate H_2.[17,18,34,35,91] The mechanism of electrocatalytic H_2 production by $[Co^{II}(L2)(CH_3CN)]^{2+}$ that is presented in Scheme 1 is qualitatively similar to this mechanism in the sense that protonation of $[HCo^{II}(L2)(CH_3CN)]^+$ results in H_2 formation. However, the mechanism of H_2 production from $[Co^{II}(L2)(CH_3CN)]^{2+}$ is distinct since the pendant amines of the **L2** ligand serve as proton relays to lower the kinetic barrier for proton delivery from the bulk solution to the cobalt, which results in fast catalytic rates. The cobalt "hangman" porphyrin catalyst reported by Nocera et al. features a pendant carboxylic acid group that facilitates an *intra*molecular proton-coupled electron transfer at the Co$^{I/0}$ couple, which results in a lower overpotential for H_2 production relative to a similar catalyst that does not possess a pendant carboxylic acid group.[18] However, the hangman carboxylic acid has not been demonstrated to increase the rate of H_2 formation by facilitating *inter*molecular proton transfer from an acid substrate to the cobalt. Recent studies on cobalt catalysts containing either a macrocylic diimine-dioxime ligand[10,92] or 1,2-dithiolene ligands[93] have indicated that ligand protonation is likely to play a role in electrocatalytic H_2 production, though it is not yet clear for either of these catalysts whether intramolecular proton transfer from the ligands to cobalt improves the rates of catalysis.

To the best of our knowledge, the experimental TOF of 18,000 s^{-1} for $[Co^{II}(L2)(CH_3CN)]^{2+}$ is the fastest rate of electrocatalytic H_2 production measured for a molecular cobalt catalyst. It is important to note that this TOF corresponds to a rate-limiting isomerization step measured under pseudo-zero order conditions at a high concentration of acid (>400 mM). Large first-order rate constants have been reported for other cobalt catalysts,[9,13,17,94] though these rate constants are typically measured at low acid concentrations (<50 mM) where the observed TOF is much less than 18,000 s^{-1}. For example, a second-order rate constant of 7×10^6 M^{-1} s^{-1} has been reported for protonation of a cobalt(bisiminopyridine) electrocatalyst by H_3O^+ in aqueous solution at pH $\geq$ 4.[13] The hydronium concentration is 0.1 mM for an aqueous solution at pH = 4, which would correspond to an observed rate constant (k_{obs} or TOF) of 700 s^{-1} for H_2 production by the cobalt(bisiminopyridine) electrocatalyst under these conditions.

dx.doi.org/10.1021/ic4025475 | Inorg. Chem. 2013, 52, 14391−14403

CONCLUSIONS

The complexes $[Co^{II}(L2)(CH_3CN)]^{2+}$ and $[Co^{II}(L3)(CH_3CN)]^{2+}$ are active electrocatalysts for H_2 production using 1:1 $[(DMF)H]^+$:DMF in acetonitrile solution. Experimental and computational thermochemical studies indicate that under conditions of fast catalysis (18,000 s^{-1}) H_2 elimination likely occurs from *endo*-$[HCo^{II}(L2\text{-}H)(CH_3CN)]^+$, where the ligand proton is located on a pendant amine adjacent to the hydride ligand. However, exo protonation of $[HCo^{II}(L2)(CH_3CN)]^+$ is kinetically preferred over endo protonation, and the net intramolecular isomerization of the nonproductive *exo*-$[HCo^{II}(L2\text{-}H)(CH_3CN)]^+$ isomer to *endo*-$[HCo^{II}(L2\text{-}H)(CH_3CN)]^+$ is believed to be rate-limiting for catalysis. Notably, protonation of $[HCo^{II}(L2)(CH_3CN)]^+$ is faster than acetonitrile dissociation from $[HCo^{II}(L2)(CH_3CN)]^+$ (1000 s^{-1}), and therefore reduction of $[HCo^{II}(L2)]^+$ to $HCo^{I}(L2)$ is not expected to occur under conditions in which rapid H_2 formation is observed. These results highlight the importance of precise delivery of protons to achieve fast rates of H_2 production catalysis, and the value of thermochemical studies to understand reactivity and rationally design new catalysts.

EXPERIMENTAL SECTION

Methods and Materials. All manipulations were carried out under N_2 using standard vacuum line, Schlenk, and inert-atmosphere glovebox techniques. Acetonitrile (Alfa-Aesar, anhydrous, amine-free) was purified by sparging with N_2 and passage through neutral alumina using an Innovative Technology, Inc., Pure Solv solvent purification system. Dimethylformamide (Burdick & Jackson) was dried over neutral alumina and filtered. Acetonitrile-d_3 (Cambridge Isotope Laboratories) was vacuum-distilled from P_2O_5. Tetrabutylammonium hexafluorophosphate (Fluka, ≥99%) was used as received. Tetraethylammonium tetrafluoroborate (Alfa-Aesar) was recrystallized twice from CH_3CN/Et_2O and dried under vacuum at room temperature. Trifluoromethanesulfonic acid (Aldrich, 99%) was used as received and handled under nitrogen. Dimethylformamide-trifluoromethanesulfonic acid, $[(DMF)H]^+$, was prepared by the method of Favier and Duñach.[95] Anilinium salts were prepared by reaction of the substituted aniline with 1.5 equiv of $HBF_4{\cdot}Et_2O$ or triflic acid followed by recrystallization from CH_3CN/Et_2O. Water was dispensed from a Millipore Milli-Q purifier and sparged with nitrogen. Ferrocene (Aldrich) was sublimed under vacuum before use. 2,4,6-Trimethylpyridine (Aldrich, 97%) was degassed via 3 consecutive freeze−pump−thaw cycles and dried over 4 Å molecular sieves. *p*-Bromoaniline (Aldrich, 97%), 2,6-dichloroaniline (Aldrich, 98%), and 2,4,6-trichloroaniline (Alfa Aesar, 98%) were used as received. The complexes $[Co^{II}(L2)(CH_3CN)](BF_4)_2$, $[Co^{II}(L3)(CH_3CN)](BF_4)_2$, $[HCo^{III}(L2)(CH_3CN)](BF_4)_2$, and $[HCo^{III}(L3)(CH_3CN)](BF_4)_2$ were prepared according to literature procedures.[40] The ^{15}N-labeled L2 ligand and its corresponding cobalt complexes were prepared analogously to the unlabeled derivatives by using ^{15}N-labeled aniline (Cambridge Isotope Laboratories, 98%).

Instrumentation. ^1H, ^{15}N, and ^{31}P NMR spectra were recorded on a Varian Inova or NMR S spectrometer (500 MHz for ^1H) at 25 °C. All ^1H chemical shifts have been internally calibrated to the monoprotio impurity of the deuterated solvent. The ^{31}P NMR spectra were referenced to external phosphoric acid at 0 ppm. The ^{15}N NMR spectra were referenced to external aqueous $^{15}NH_4{}^{15}NO_3$, with the $^{15}NO_3^-$ resonance set at −4 ppm relative to nitromethane at 0 ppm. NMR simulations were performed using the line-fitting feature of MestReNova v6.0.4.

Voltammetry measurements were performed using a CH Instruments 620D potentiostat equipped with a standard three-electrode cell. Experiments were performed in a glovebox at ambient temperature, 23 ± 2 °C, using a 3−5 mL conical glass vial fitted with a polysilicone cap having openings sized to closely accept each electrode. The working electrode (1 mm PEEK-encased glassy carbon disc, Cypress Systems EE040) was polished using diamond paste (Buehler, 0.25 μm) on a polishing pad wet with purified H_2O (vide infra), then the electrode was rinsed with neat acetonitrile. A glassy carbon rod (Structure Probe, Inc.) was used as the counter-electrode, and a silver wire suspended in a solution of Bu_4NPF_6 (0.2 M) in acetonitrile and separated from the analyte solution by a Vycor frit (CH Instruments 112) was used a pseudo-reference electrode. Ferrocene was used as an internal standard, and all potentials are referenced to the ferrocenium/ferrocene couple at 0 V. Controlled potential electrolyses were performed using a CH Instruments 1100A power potentiostat. Gas analysis for H_2 was performed using an Agilent 6850 gas chromatograph fitted with a 10 ft long Supelco 1/8" Carbosieve 100/120 column, calibrated with two H_2/N_2 gas mixtures of known composition.

Computational Details. All structures were optimized without symmetry constraints using the B3P86[96,97] functional. The Stuttgart basis set with effective core potential (ECP)[98] was used for the Co atom, whereas the 6-31G* basis set[99,100] was used for all other atoms with one additional *p* polarization funtion [$\xi(p) = 1.1$] for the hydride ligands and the protons located on a pendant amine. Each structure was confirmed by a frequency calculation at the same level of theory to be a real local minimum on the potential energy surface without imaginary frequency. For each species, the gas phase free energy was calculated at 298 K in the harmonic approximation. Solvation free energies in acetonitrile were calculated by using the polarizable continuum model (C-PCM)[101,102] using Bondi[103] atomic radii. This computational setup has been shown to accurately predict thermodynamic properties of $[Ni(diphosphine)_2]^{2+}$ complexes[59] and to describe the H_2 chemistry of the $Ni(P_2N_2)_2$ complexes.[73] All of the calculations were carried out with the program Gaussian 09.[104]

Catalytic Hydrogen Production. *Determination of Overpotential and Rate.* A scan rate of 0.5 V s^{-1} was used for all experiments with 1:1 $[(DMF)H]^+$:DMF as the acid, and a scan rate of 0.05 V s^{-1} was used for all experiments with *p*-bromoanilinium as the acid. Overpotentials were taken as the difference between the half-wave potential of the catalytic wave and the thermodynamic potential, $E°$, for the reduction of acid to free base plus one-half equivalent H_2 gas. At each acid concentration, i_p was measured directly from the $Co^{II/I}$ couple. The potentials at which i_{cat} values were measured were located by finding the most positive potential of each catalytic wave beyond the half-peak potential for which the second derivative of the *i* vs *E* trace is approximately constant. Calibration curves for the background reduction of the acid by the working electrode were constructed, and all i_{cat} values were corrected for the background current passed at the same potential and acid concentration. Reported rates are the average of 2−3 separate determinations. A representative experiment is given below.

Using $[Co^{II}(L2)(CH_3CN)]^{2+}$ as Catalyst and 1:1 $[(DMF)H]^+$:DMF as Acid. A 0.5 mM solution of $[Co^{II}(L2)(CH_3CN)]^{2+}$ in acetonitrile (0.2 M Bu_4NPF_6) was prepared, and a baseline voltammogram was recorded at a scan rate of 500 mV s^{-1}. Aliquots of a 1.5 M 1:1 $[(DMF)H]^+$:DMF solution in acetonitrile (0.2 M Bu_4NPF_6) were added via microsyringe in 50−200 μL increments until a final acid concentration of 500−600 mM was obtained. After each addition of acid, the working electrode was cleaned by polishing (vide supra), and a voltammogram was recorded. Subsequent to the completion of acid additions, the described method was repeated using purified H_2O. H_2O was added by microsyringe in 5−40 μL increments until the observed catalytic current remained constant.

Order with Respect to Cobalt. A 2.36 mL acetonitrile solution containing $[Co^{II}(L3)(CH_3CN)]^{2+}$ (0.3 mM), *p*-bromoanilinium triflate (0.27 M), water (0.36 M), and NBu_4PF_6 (0.2 M) was obtained upon completion of a typical acid concentration dependence experiment. Aliquots of a 21 mM solution of $[Co^{II}(L3)(CH_3CN)]^{2+}$ in acetonitrile were added via microsyringe in 20 μL increments. After each addition of catalyst, the working electrode was cleaned by polishing (vide supra), and a voltammogram was recorded at a scan rate of 0.05 V s^{-1}.

Controlled Potential Coulometry. A five-necked flask having a total volume of 500 mL was used as the bulk electrolysis vessel and was assembled in a glovebox. Three of the necks were 24/40 ground glass joints, one of which was a rubber septum pierced with a copper wire

dx.doi.org/10.1021/ic4025475 | Inorg. Chem. 2013, 52, 14391−14403

attached to a 1 mm PEEK-encased glassy carbon disc electrode for CV measurements. A second neck was equipped with a cylinder of reticulated vitreous carbon as a working electrode for bulk electrolysis. The third neck was equipped with a 13 mm glass tube terminating in an ultrafine glass filter disk and filled with acetonitrile (0.2 M NEt_4BF_4) and a Nichrome wire as a counter electrode. The final two necks were threaded glass joints, one of which was fit with a 7 mm glass tube terminating in a Vycor fritted disk and filled with acetonitrile (0.2 M NEt_4BF_4) and a silver wire as a reference electrode, while the final neck was sealed with a threaded stopper. With these fittings attached, the cell had a total volume of 299 mL. The cell was filled with 25 mL of an acetonitrile solution containing $[Co^{II}(L3)(CH_3CN)]^{2+}$ (12.6 mg, 0.0123 mmol, 0.5 mM), $[(DMF)H]^+$ (1.401 g, 6.28 mmol, 0.25 M), DMF (0.48 mL, 6.2 mmol, 0.25 M), NEt_4BF_4 (1.10 g, 5.1 mmol, 0.2 M), and ferrocene (4.7 mg, 0.025 mmol, 1.0 mM). Controlled-potential coulometry was performed at −1.4 V versus the ferrocenium/ferrocene internal reference. After 25.2 C of charge was passed, a 500 μL sample of the headspace gas was removed using a gastight syringe, then 100 μL of the sample was analyzed by gas chromatography using the detector response calibration to determine the amount of H_2. The percentage of hydrogen and nitrogen in the headspace were determined through calibration against gas standards of known composition. The total amount of hydrogen produced was calculated as the sum of the hydrogen in the headspace and the sum of the hydrogen dissolved in the solvent, as determined from Henry's Law.[105] Using the moles of H_2 produced (0.132 mmol) and the charge passed (25.2 C), a current efficiency of 101 ± 5% was calculated for H_2 production.

Protonation of $[HCo^{III}(L2)(CH_3CN)]^{2+}$. A drop (excess) of HBF_4·Et_2O was added by syringe to a CD_3CN solution of $[HCo^{III}(L2)(CH_3CN)]^{2+}$, then NMR spectra were recorded after 50 min. The major product observed by NMR spectroscopy was assigned as *exo*-$[HCo^{III}(L2\text{-}H)(CH_3CN)]^{2+}$ based on the spectroscopic data given below. A hydride resonance of a minor product was observed by ^{1}H NMR spectroscopy at −14.2 ppm, though other resonances could not be observed for this product. ^{1}H NMR (500 MHz, CD_3CN): δ 12.20 (s, 1H, N*H*N), 7.73−7.36 (m, 26H, Ar*H*), 6.60 (dd, 2H, $^3J_{HP}$ = 10.0 Hz, $^3J_{HH}$ = 7.6 Hz, Ar*H*), 5.07 (m, 2H, PCH_2N), 4.99 (m, 2H, PCH_2N), 4.32 (d, 2H, $^2J_{HH}$ = 12.3 Hz, PCH_2N), 4.22 (d, 2H, $^2J_{HH}$ = 13.5 Hz, PCH_2N), 3.34 (m, 2H, P$(CH_2)_2$P), 2.89 (m, 2H, P$(CH_2)_2$P), 2.62 (m, 4H, P$(CH_2)_2$P), 1.92 (s, CH_3CN), −21.82 (br s, $\Delta\nu_{1/2}$ = 177 Hz, 1H, Co*H*). ^{31}P{^{1}H} NMR (CD_3CN): δ 76 (br s, $\Delta\nu_{1/2}$ = 1425 Hz, 2P), 60 (br s, $\Delta\nu_{1/2}$ = 1014 Hz, 2P). For the ^{15}N-labeled complex, ^{1}H NMR (500 MHz, CD_3CN): δ 12.22 (dd, 1H, $^1J_{NH}$ = 41.5, 30.5 Hz, N*H*N). ^{15}N NMR (51 MHz, CD_3CN): δ −321.4 (d, $^1J_{NH}$ = 39.9 Hz), −323.1 (d, $^1J_{NH}$ = 28.9 Hz).

pK_a Determinations. Analytes were equilibrated with an appropriate acid or base reference in CD_3CN solution and monitored by ^{1}H NMR spectroscopy. Averaged resonances were observed for the protonated and deprotonated forms of the analyte, as well as for the protonated and deprotonated forms of the reference, unless noted otherwise. The weighted average of the chemical shifts of the protonated and deprotonated forms were used to determine the ratio of each for the analyte as well as the reference. Listed errors are three times the standard deviation.

$[HCo^{III}(L2)(CH_3CN)]^{2+}$. The p$K_a$ value for $[HCo^{III}(L2)(CH_3CN)]^{2+}$ was determined against 2,4,6-trimethylpyridine (pK_a = 14.98)[49] using three different ratios of analyte (<9 mM) and reference (<40 mM) over 1−2 days to verify that equilibrium was attained. Separate resonances were observed for $[HCo^{III}(L2)(CH_3CN)]^{2+}$ and for $[Co^{I}(L2)(CH_3CN)]^+$, and the ratio of the cobalt species was determined by integration. The experiment was repeated, and a K_{eq} value of 0.10 ± 0.02 was calculated from the six measurements. A pK_a value of 16.0 ± 0.4 was determined for $[HCo^{III}(L2)(CH_3CN)]^{2+}$.

2,4,6-Trichloroanilinium. The pK_a value for 2,4,6-trichloroanilinium was determined by equilibration with 2,6-dichloroanilinium (pK_a^{MeCN} = 5.06).[49] Three solutions were prepared of 2,4,6-trichloroaniline and 2,6-dichloroanilinium in ratios of 2:1, 1:1, and 1:2, with concentrations of the analyte and reference at less than 15 mM. A K_{eq} value of 6.9 ± 0.8 was calculated from these measurements, and a pK_a value of 4.2 ± 0.1 was determined for 2,4,6-trichloroanilinium.

$[HCo^{III}(L2\text{-}H)(CH_3CN)]^{3+}$. The p$K_a$ value for *exo*-$[HCo^{III}(L2\text{-}H)(CH_3CN)]^{3+}$ was determined using $[HCo^{III}(L2)(CH_3CN)]^{2+}$ as the analyte (<17 mM) and 2,4,6-trichloroanilinium tetrafluoroborate (pK_a = 4.2) as the reference (≤400 mM). Six different ratios of analyte and reference were allowed to equilibrate for 30 min. A K_{eq} value of 0.21 ± 0.04 was calculated from the six measurements, and a pK_a value of 3.5 ± 0.4 was determined for $[HCo^{III}(L2\text{-}H)(CH_3CN)]^{3+}$.

■ ASSOCIATED CONTENT

Ⓢ Supporting Information

Experimental details, cyclic voltammograms, plots of k_{obs} versus acid concentration, NMR spectra, alternate electrocatalytic cycle, example thermochemical cycles, additional details of computational isodesmic reactions, energies and coordinates from DFT computations. This material is available free of charge via the Internet at http://pubs.acs.org.

■ AUTHOR INFORMATION

Corresponding Authors

*E-mail: eric.wiedner@pnnl.gov (E.S.W.).

*E-mail: morris.bullock@pnnl.gov (R.M.B.).

Notes

The authors declare no competing financial interest.

■ ACKNOWLEDGMENTS

We thank Dr. Shentan Chen for many helpful discussions. This research was supported as part of the Center for Molecular Electrocatalysis, an Energy Frontier Research Center funded by the U.S. Department of Energy, Office of Science, Office of Basic Energy Sciences. Computational resources were provided at the National Energy Research Scientific Computing Center (NERSC) at Lawrence Berkeley National Laboratory. Pacific Northwest National Laboratory is operated by Battelle for the U.S. Department of Energy.

■ REFERENCES

(1) Artero, V.; Chavarot-Kerlidou, M.; Fontecave, M. *Angew. Chem., Int. Ed.* **2011**, *50*, 7238−7266.

(2) Dempsey, J. L.; Brunschwig, B. S.; Winkler, J. R.; Gray, H. B. *Acc. Chem. Res.* **2009**, *42*, 1995−2004.

(3) Eckenhoff, W. T.; McNamara, W. R.; Du, P.; Eisenberg, R. *Biochim. Biophys. Acta, Bioenerg.* **2013**, *1827*, 958−973.

(4) Wang, M.; Chen, L.; Sun, L. *Energy Environ. Sci.* **2012**, *5*, 6763−6778.

(5) Koelle, U.; Ohst, S. *Inorg. Chem.* **1986**, *25*, 2689−2694.

(6) Hu, X. L.; Cossairt, B. M.; Brunschwig, B. S.; Lewis, N. S.; Peters, J. C. *Chem. Commun.* **2005**, 4723−4725.

(7) Razavet, M.; Artero, V.; Fontecave, M. *Inorg. Chem.* **2005**, *44*, 4786−4795.

(8) Baffert, C.; Artero, V.; Fontecave, M. *Inorg. Chem.* **2007**, *46*, 1817−1824.

(9) Hu, X. L.; Brunschwig, B. S.; Peters, J. C. *J. Am. Chem. Soc.* **2007**, *129*, 8988−8998.

(10) Jacques, P. A.; Artero, V.; Pecaut, J.; Fontecave, M. *Proc. Natl. Acad. Sci. U.S.A.* **2009**, *106*, 20627−20632.

(11) Berben, L. A.; Peters, J. C. *Chem. Commun.* **2010**, *46*, 398−400.

(12) McCrory, C. C. L.; Uyeda, C.; Peters, J. C. *J. Am. Chem. Soc.* **2012**, *134*, 3164−3170.

(13) Stubbert, B. D.; Peters, J. C.; Gray, H. B. *J. Am. Chem. Soc.* **2011**, *133*, 18070−18073.

(14) Valdez, C. N.; Dempsey, J. L.; Brunschwig, B. S.; Winkler, J. R.; Gray, H. B. *Proc. Natl. Acad. Sci. U.S.A.* **2012**, *109*, 15589−15593.

(15) Sun, Y.; Bigi, J. P.; Piro, N. A.; Tang, M. L.; Long, J. R.; Chang, C. J. *J. Am. Chem. Soc.* **2011**, *133*, 9212−9215.

(16) Nippe, M.; Khnayzer, R. S.; Panetier, J. A.; Zee, D. Z.; Olaiya, B. S.; Head-Gordon, M.; Chang, C. J.; Castellano, F. N.; Long, J. R. *Chem. Sci.* **2013**, *4*, 3934−3945.
(17) Marinescu, S. C.; Winkler, J. R.; Gray, H. B. *Proc. Natl. Acad. Sci. U.S.A.* **2012**, *109*, 15127−15131.
(18) Lee, C. H.; Dogutan, D. K.; Nocera, D. G. *J. Am. Chem. Soc.* **2011**, *133*, 8775−8777.
(19) McNamara, W. R.; Han, Z.; Alperin, P. J.; Brennessel, W. W.; Holland, P. L.; Eisenberg, R. *J. Am. Chem. Soc.* **2011**, *133*, 15368−15371.
(20) McNamara, W. R.; Han, Z. J.; Yin, C. J.; Brennessel, W. W.; Holland, P. L.; Eisenberg, R. *Proc. Natl. Acad. Sci. U.S.A.* **2012**, *109*, 15594−15599.
(21) Hawecker, J.; Lehn, J. M.; Ziessel, R. *New J. Chem.* **1983**, *7*, 271−277.
(22) Fihri, A.; Artero, V.; Pereira, A.; Fontecave, M. *Dalton Trans.* **2008**, 5567−5569.
(23) Fihri, A.; Artero, V.; Razavet, M.; Baffert, C.; Leibl, W.; Fontecave, M. *Angew. Chem., Int. Ed.* **2008**, *47*, 564−567.
(24) Du, P.; Schneider, J.; Luo, G.; Brennessel, W. W.; Eisenberg, R. *Inorg. Chem.* **2009**, *48*, 4952−4962.
(25) Lazarides, T.; McCormick, T.; Du, P.; Luo, G.; Lindley, B.; Eisenberg, R. *J. Am. Chem. Soc.* **2009**, *131*, 9192−9194.
(26) Probst, B.; Rodenberg, A.; Guttentag, M.; Hamm, P.; Alberto, R. *Inorg. Chem.* **2010**, *49*, 6453−6460.
(27) Probst, B.; Guttentag, M.; Rodenberg, A.; Hamm, P.; Alberto, R. *Inorg. Chem.* **2011**, *50*, 3404−3412.
(28) Singh, W. M.; Baine, T.; Kudo, S.; Tian, S.; Ma, X. A. N.; Zhou, H.; DeYonker, N. J.; Pham, T. C.; Bollinger, J. C.; Baker, D. L.; Yan, B.; Webster, C. E.; Zhao, X. *Angew. Chem., Int. Ed.* **2012**, *51*, 5941−5944.
(29) Sun, Y.; Sun, J.; Long, J. R.; Yang, P.; Chang, C. J. *Chem. Sci.* **2013**, *4*, 118−124.
(30) Du, P.; Eisenberg, R. *Energy Environ. Sci.* **2012**, *5*, 6012−6021.
(31) Zhang, P.; Jacques, P. A.; Chavarot-Kerlidou, M.; Wang, M.; Sun, L.; Fontecave, M.; Artero, V. *Inorg. Chem.* **2012**, *51*, 2115−2120.
(32) Li, L.; Duan, L.; Wen, F.; Li, C.; Wang, M.; Hagfeldt, A.; Sun, L. *Chem. Commun.* **2012**, *48*, 988−990.
(33) Huang, J.; Mulfort, K. L.; Du, P.; Chen, L. X. *J. Am. Chem. Soc.* **2012**, *134*, 16472−16475.
(34) Solis, B. H.; Hammes-Schiffer, S. *Inorg. Chem.* **2011**, *50*, 11252−11262.
(35) Muckerman, J. T.; Fujita, E. *Chem. Commun.* **2011**, *47*, 12456−12458.
(36) King, A. E.; Surendranath, Y.; Piro, N. A.; Bigi, J. P.; Long, J. R.; Chang, C. J. *Chem. Sci.* **2013**, *4*, 1578−1587.
(37) Wiedner, E. S.; Yang, J. Y.; Dougherty, W. G.; Kassel, W. S.; Bullock, R. M.; Rakowski DuBois, M.; DuBois, D. L. *Organometallics* **2010**, *29*, 5390−5401.
(38) Jacobsen, G. M.; Yang, J. Y.; Twamley, B.; Wilson, A. D.; Bullock, R. M.; Rakowski DuBois, M.; DuBois, D. L. *Energy Environ. Sci.* **2008**, *1*, 167−174.
(39) Wiedner, E. S.; Yang, J. Y.; Chen, S. T.; Raugei, S.; Dougherty, W. G.; Kassel, W. S.; Helm, M. L.; Bullock, R. M.; Rakowski DuBois, M.; DuBois, D. L. *Organometallics* **2012**, *31*, 144−156.
(40) Wiedner, E. S.; Roberts, J. A. S.; Dougherty, W. G.; Kassel, W. S.; DuBois, D. L.; Bullock, R. M. *Inorg. Chem.* **2013**, *52*, 9975−9988.
(41) Izutsu, K. *Acid-Base Dissociation Constants in Dipolar Aprotic Solvents*; Blackwell Scientific Publications: Oxford, U.K., 1990.
(42) Kolthoff, I. M.; Chantooni, M. K.; Bhowmik, S. *Anal. Chem.* **1967**, *39*, 1627−1633.
(43) Nicholson, R. S.; Shain, I. *Anal. Chem.* **1964**, *36*, 706−723.
(44) Savéant, J. M.; Vianello, E. *Electrochim. Acta* **1965**, *10*, 905−920.
(45) Savéant, J. M.; Vianello, E. *Electrochim. Acta* **1967**, *12*, 629−646.
(46) Pool, D. H.; DuBois, D. L. *J. Organomet. Chem.* **2009**, *694*, 2858−2865.
(47) Bard, A. J.; Faulkner, L. R. *Electrochemical Methods: Fundamentals and Applications*, 2nd ed.; John Wiley & Sons: Hoboken, NJ, 2001.
(48) Roberts, J. A. S.; Bullock, R. M. *Inorg. Chem.* **2013**, *52*, 3823−3835.
(49) Kaljurand, I.; Kutt, A.; Soovali, L.; Rodima, T.; Maemets, V.; Leito, I.; Koppel, I. A. *J. Org. Chem.* **2005**, *70*, 1019−1028.
(50) Ciancanelli, R.; Noll, B. C.; DuBois, D. L.; Rakowski DuBois, M. *J. Am. Chem. Soc.* **2002**, *124*, 2984−2992.
(51) The thermochemical values of this cobalt complex were corrected using an updated value for the pK_a of anisidinium, which was used to measure the pK_a of the cobalt(III) hydride complex. Details of this correction are given in the Supporting Information.
(52) Wayner, D. D. M.; Parker, V. D. *Acc. Chem. Res.* **1993**, *26*, 287−294.
(53) Parker, V. D.; Handoo, K. L.; Roness, F.; Tilset, M. *J. Am. Chem. Soc.* **1991**, *113*, 7493−7498.
(54) Tilset, M.; Parker, V. D. *J. Am. Chem. Soc.* **1989**, *111*, 6711−6717; as modified in *J. Am. Chem. Soc.* **1990**, *112*, 2843.
(55) Appel, A. M.; Lee, S. J.; Franz, J. A.; DuBois, D. L.; Rakowski DuBois, M. *J. Am. Chem. Soc.* **2009**, *131*, 5224−5232.
(56) Appel, A. M.; Lee, S. J.; Franz, J. A.; DuBois, D. L.; Rakowski DuBois, M.; Twamley, B. *Organometallics* **2009**, *28*, 749−754.
(57) Roberts, J. A. S.; Appel, A. M.; DuBois, D. L.; Bullock, R. M. *J. Am. Chem. Soc.* **2011**, *133*, 14604−14613.
(58) Tilset, M. *Inorg. Chem.* **1994**, *33*, 3121−3126.
(59) Chen, S.; Rousseau, R.; Raugei, S.; Dupuis, M.; DuBois, D. L.; Bullock, R. M. *Organometallics* **2011**, *30*, 6108−6118.
(60) Bianchini, C.; Mealli, C.; Meli, A.; Peruzzini, M.; Zanobini, F. *J. Am. Chem. Soc.* **1988**, *110*, 8725−8726.
(61) Bianchini, C.; Mealli, C.; Peruzzini, M.; Zanobini, F. *J. Am. Chem. Soc.* **1992**, *114*, 5905−5906.
(62) Heinekey, D. M.; Liegeois, A.; van Roon, M. *J. Am. Chem. Soc.* **1994**, *116*, 8388−8389.
(63) Heinekey, D. M.; van Roon, M. *J. Am. Chem. Soc.* **1996**, *118*, 12134−12140.
(64) Mock, M. T.; Potter, R. G.; O'Hagan, M. J.; Camaioni, D. M.; Dougherty, W. G.; Kassel, W. S.; DuBois, D. L. *Inorg. Chem.* **2011**, *50*, 11914−11928.
(65) Rossin, A.; Caporali, M.; Gonsalvi, L.; Guerri, A.; Lledós, A.; Peruzzini, M.; Zanobini, F. *Eur. J. Inorg. Chem.* **2009**, *2009*, 3055−3059.
(66) Findlater, M.; Bernskoetter, W. H.; Brookhart, M. *J. Am. Chem. Soc.* **2010**, *132*, 4534−4535.
(67) Rybtchinski, B.; Ben-David, Y.; Milstein, D. *Organometallics* **1997**, *16*, 3786−3793.
(68) Romero, P. E.; Whited, M. T.; Grubbs, R. H. *Organometallics* **2008**, *27*, 3422−3429.
(69) Kloek, S. M.; Heinekey, D. M.; Goldberg, K. I. *Organometallics* **2006**, *25*, 3007−3011.
(70) Wilson, A. D.; Shoemaker, R. K.; Miedaner, A.; Muckerman, J. T.; DuBois, D. L.; Rakowski DuBois, M. *Proc. Natl. Acad. Sci. U.S.A.* **2007**, *104*, 6951−6956.
(71) Appel, A. M.; Pool, D. H.; O'Hagan, M.; Shaw, W. J.; Yang, J. Y.; Rakowski DuBois, M.; DuBois, D. L.; Bullock, R. M. *ACS Catal.* **2011**, *1*, 777−785.
(72) Jacobsen, G. M.; Shoemaker, R. K.; McNevin, M. J.; Rakowski DuBois, M.; DuBois, D. L. *Organometallics* **2007**, *26*, 5003−5009.
(73) Chen, S.; Raugei, S.; Rousseau, R.; Dupuis, M.; Bullock, R. M. *J. Phys. Chem. A* **2010**, *114*, 12716−12724.
(74) Stewart, M. P.; Ho, M.-H.; Wiese, S.; Lindstrom, M. L.; Thogerson, C. E.; Raugei, S.; Bullock, R. M.; Helm, M. L. *J. Am. Chem. Soc.* **2013**, *135*, 6033−6046.
(75) Custelcean, R.; Jackson, J. E. *Chem. Rev.* **2001**, *101*, 1963−1980.
(76) Hebden, T. J.; St. John, A. J.; Gusev, D. G.; Kaminsky, W.; Goldberg, K. I.; Heinekey, D. M. *Angew. Chem., Int. Ed.* **2011**, *50*, 1873−1876.
(77) Raebiger, J. W.; Miedaner, A.; Curtis, C. J.; Miller, S. M.; Anderson, O. P.; DuBois, D. L. *J. Am. Chem. Soc.* **2004**, *126*, 5502−5514.
(78) Berning, D. E.; Noll, B. C.; DuBois, D. L. *J. Am. Chem. Soc.* **1999**, *121*, 11432−11447.
(79) Nimlos, M. R.; Chang, C. H.; Curtis, C. J.; Miedaner, A.; Pilath, H. M.; DuBois, D. L. *Organometallics* **2008**, *27*, 2715−2722.
(80) Qi, X.-J.; Liu, L.; Fu, Y.; Guo, Q.-X. *Organometallics* **2006**, *25*, 5879−5886.

(81) Mock, M. T.; Potter, R. G.; Camaioni, D. M.; Li, J.; Dougherty, W. G.; Kassel, W. S.; Twamley, B.; DuBois, D. L. *J. Am. Chem. Soc.* **2009**, *131*, 14454−14465.
(82) DuBois, D. L.; Blake, D. M.; Miedaner, A.; Curtis, C. J.; Rakowski DuBois, M.; Franz, J. A.; Linehan, J. C. *Organometallics* **2006**, *25*, 4414−4419.
(83) Price, A. J.; Ciancanelli, R.; Noll, B. C.; Curtis, C. J.; DuBois, D. L.; Rakowski DuBois, M. *Organometallics* **2002**, *21*, 4833−4839.
(84) Fraze, K.; Wilson, A. D.; Appel, A. M.; Rakowski DuBois, M.; DuBois, D. L. *Organometallics* **2007**, *26*, 3918−3924.
(85) O'Hagan, M.; Shaw, W. J.; Raugei, S.; Chen, S.; Yang, J. Y.; Kilgore, U. J.; DuBois, D. L.; Bullock, R. M. *J. Am. Chem. Soc.* **2011**, *133*, 14301−14312.
(86) Hulley, E. B.; Welch, K. D.; Appel, A. M.; DuBois, D. L.; Bullock, R. M. *J. Am. Chem. Soc.* **2013**, *135*, 11736−11739.
(87) Henry, R. M.; Shoemaker, R. K.; DuBois, D. L.; Rakowski DuBois, M. *J. Am. Chem. Soc.* **2006**, *128*, 3002−3010.
(88) O'Hagan, M.; Ho, M.-H.; Yang, J. Y.; Appel, A. M.; Rakowski DuBois, M.; Raugei, S.; Shaw, W. J.; DuBois, D. L.; Bullock, R. M. *J. Am. Chem. Soc.* **2012**, *134*, 19409−19424.
(89) Kilgore, U. J.; Roberts, J. A. S.; Pool, D. H.; Appel, A. M.; Stewart, M. P.; Rakowski DuBois, M.; Dougherty, W. G.; Kassel, W. S.; Bullock, R. M.; DuBois, D. L. *J. Am. Chem. Soc.* **2011**, *133*, 5861−5872.
(90) Kilgore, U. J.; Stewart, M. P.; Helm, M. L.; Dougherty, W. G.; Kassel, W. S.; Rakowski DuBois, M.; DuBois, D. L.; Bullock, R. M. *Inorg. Chem.* **2011**, *50*, 10908−10918.
(91) Dempsey, J. L.; Winkler, J. R.; Gray, H. B. *J. Am. Chem. Soc.* **2010**, *132*, 16774−16776.
(92) Solis, B. H.; Yu, Y.; Hammes-Schiffer, S. *Inorg. Chem.* **2013**, *52*, 6994−6999.
(93) Solis, B. H.; Hammes-Schiffer, S. *J. Am. Chem. Soc.* **2012**, *134*, 15253−15256.
(94) Szajna-Fuller, E.; Bakac, A. *Eur. J. Inorg. Chem.* **2010**, *2010*, 2488−2494.
(95) Favier, I.; Duñach, E. *Tetrahedron Lett.* **2004**, *45*, 3393−3395.
(96) Becke, A. D. *J. Chem. Phys.* **1993**, *98*, 5648−5652.
(97) Perdew, J. P. *Phys. Rev. B* **1986**, *33*, 8822−8824.
(98) Andrae, D.; Haussermann, U.; Dolg, M.; Stoll, H.; Preuss, H. *Theor. Chem. Acc.* **1990**, *77*, 123−141.
(99) Francl, M. M.; Pietro, W. J.; Hehre, W. J.; Binkley, J. S.; Gordon, M. S.; Defrees, D. J.; Pople, J. A. *J. Chem. Phys.* **1982**, *77*, 3654−3665.
(100) Rassolov, V. A.; Ratner, M. A.; Pople, J. A.; Redfern, P. C.; Curtiss, L. A. *J. Comput. Chem.* **2001**, *22*, 976−984.
(101) Barone, V.; Cossi, M. *J. Phys. Chem. A* **1998**, *102*, 1995−2001.
(102) Cossi, M.; Rega, N.; Scalmani, G.; Barone, V. *J. Comput. Chem.* **2003**, *24*, 669−681.
(103) Bondi, A. *J. Phys. Chem.* **1964**, *68*, 441−451.
(104) Frisch, M. J.; Trucks, G. W.; Schlegel, H. B.; Scuseria, G. E.; Robb, M. A.; Cheeseman, J. R.; Scalmani, G.; Barone, V.; Mennucci, B.; Petersson, G. A.; Nakatsuji, H.; Caricato, M.; Li, X.; Hratchian, H. P.; Izmaylov, A. F.; Bloino, J.; Zheng, G.; Sonnenberg, J. L.; Hada, M.; Ehara, M.; Toyota, K.; Fukuda, R.; Hasegawa, J.; Ishida, M.; Nakajima, T.; Honda, Y.; Kitao, O.; Nakai, H.; Vreven, T.; Montgomery, J. A., Jr.; Peralta, J. E.; Ogliaro, F.; Bearpark, M.; Heyd, J. J.; Brothers, E.; Kudin, K. N.; Staroverov, V. N.; Kobayashi, R.; Normand, J.; Raghavachari, K.; Rendell, A.; Burant, J. C.; Iyengar, S. S.; Tomasi, J.; Cossi, M.; Rega, N.; Millam, J. M.; Klene, M.; Knox, J. E.; Cross, J. B.; Bakken, V.; Adamo, C.; Jaramillo, J.; Gomperts, R.; Stratmann, R. E.; Yazyev, O.; Austin, A. J.; Cammi, R.; Pomelli, C.; Ochterski, J. W.; Martin, R. L.; Morokuma, K.; Zakrzewski, V. G.; Voth, G. A.; Salvador, P.; Dannenberg, J. J.; Dapprich, S. A.; Daniels, D.; Farkas, O.; Foresman, J. B.; Ortiz, J. V.; Cioslowski, J.; Fox, D. J. *Gaussian 09*; Revision B.01; Gaussian, Inc.: Wallingford, CT, 2009.
(105) Purwanto; Deshpande, R. M.; Chaudhari, R. V.; Delmas, H. *J. Chem. Eng. Data* **1996**, *41*, 1414−1417.